AD-A116 250 MASSACHUSETTS UNIV AMHERST ASTRONOMY RESEARCH FACILITY F/G 4/1
SCRIBE II DATA ANALYSIS.(U)
APR 82 H SAKAI, G A VANASSE F19628-81-K-0007
UNCLASSIFIED UMASS-ARF-82-323 AFGL-TR-82-0150 NL

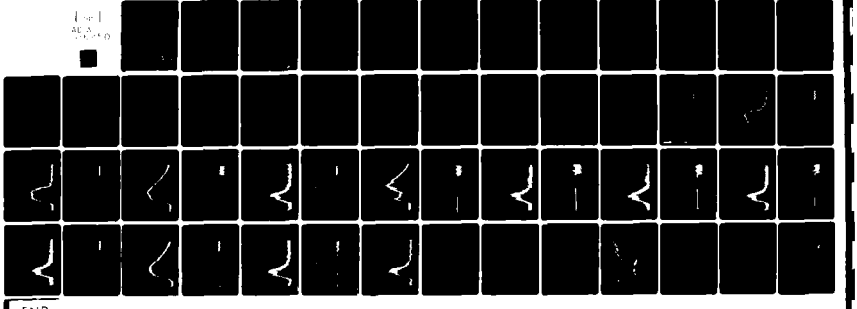

END
DATE FILMED
7-82
DTIC

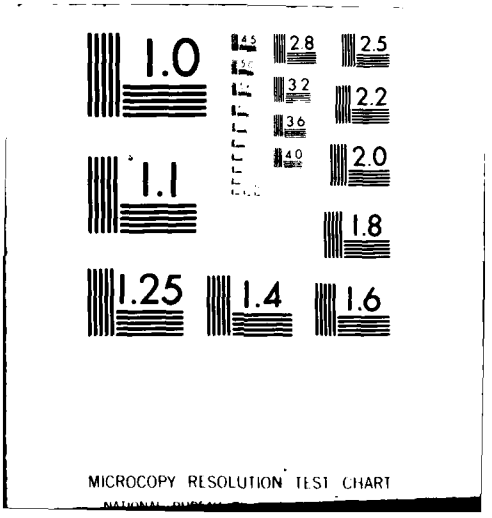
1.0
1.1
1.25
1.4
1.6
1.8
2.0
2.2
2.5
2.8
3.2
3.6
4.0
MICROCOPY RESOLUTION TEST CHART

AFGL-TR-82-0150

SCRIBE II DATA ANALYSIS

H. Sakai
G.A. Vanasse

Astronomy Research Facility
University of Massachusetts
Amherst, Massachusetts 01003

Scientific Report No. 2

April 1982

AIR FORCE GEOPHYSICS LABORATORY
AIR FORCE SYSTEMS COMMAND
UNITED STATES AIR FORCE
HANSCOM AFB, MASSACHUSETTS 01731

UNCLASSIFIED

SECURITY CLASSIFICATION OF THIS PAGE *(When Data Entered)*

REPORT DOCUMENTATION PAGE

READ INSTRUCTIONS BEFORE COMPLETING FORM

1. REPORT NUMBER: AFGL-TR-82-0150	2. GOVT ACCESSION NO.: AD-A116250
3. RECIPIENT'S CATALOG NUMBER:	
4. TITLE *(and Subtitle)*: SCRIBE II DATA ANALYSIS	5. TYPE OF REPORT & PERIOD COVERED: Scientific Report No. 2, 01 Nov 81 to 15 Apr 82
	6. PERFORMING ORG. REPORT NUMBER: UMASS-ARF-82-323
7. AUTHOR(s): H. Sakai, G.A. Vanasse*	8. CONTRACT OR GRANT NUMBER(s): F19628-81-K-0007
9. PERFORMING ORGANIZATION NAME AND ADDRESS: Astronomy Research Facility, University of Massachusetts, Amherst MA 01003	10. PROGRAM ELEMENT, PROJECT, TASK AREA & WORK UNIT NUMBERS: 61102F, 2310G4AT
11. CONTROLLING OFFICE NAME AND ADDRESS: Air Force Geophysics Laboratory, Hanscom AFB, Massachusetts 01731, Monitor: Alastair Fairbairn/OPR	12. REPORT DATE: April 1982
	13. NUMBER OF PAGES: 54
14. MONITORING AGENCY NAME & ADDRESS *(if different from Controlling Office)*	15. SECURITY CLASS. *(of this report)*: Unclassified
	15a. DECLASSIFICATION/DOWNGRADING SCHEDULE

16. DISTRIBUTION STATEMENT *(of this Report)*

Approved for public release; distribution unlimited.

17. DISTRIBUTION STATEMENT *(of the abstract entered in Block 20, if different from Report)*

18. SUPPLEMENTARY NOTES

*AFGL/OPI, Hanscom AFB, Massachusetts 01731

19. KEY WORDS *(Continue on reverse side if necessary and identify by block number)*

Atmospheric infrared emission
Atmospheric infrared transmission
Atmospheric radiance level
Cryogenic interferometer
Fourier spectroscopy
Stratosphere
Troposphere
Balloon-borne spectrometry
CO_2

20. ABSTRACT *(Continue on reverse side if necessary and identify by block number)*

The data collected by the SCRIBE October 1981 flight were analyzed. The flight history and the data obtained, centered at the 15μ CO_2 band, are summarized in this report. The down-looking spectra obtained with 0.2 cm^{-1} resolution produced no unusual features, while the horizontal-looking spectra obtained with the same resolution figure yielded remarkable findings, a continuum background feature superimposed with the molecular feature and a large variation in the radiance level at 27000 ∿ 28000 m altitude for both the molecular and the continuum feature.

DD FORM 1 JAN 73 1473 EDITION OF 1 NOV 65 IS OBSOLETE

UNCLASSIFIED

SECURITY CLASSIFICATION OF THIS PAGE *(When Data Entered)*

In the lower atmosphere, the troposphere and the stratosphere, the molecules are generally in thermal equilibrium with the local surrounding. The infrared emission resulting from this thermal excitation can be studied to determine the profile of the abundances of the molecules responsible for the emission in the atmosphere, as well as the atmospheric temperature profile. The stratospheric cryogenic balloon experiment program (SCRIBE) was developed to accomplish spectrometry of this infrared atmospheric emission with a resolution of 0.1 cm^{-1}.[1,2] The first flight took place during the month of October 1980 with partial success.[3,4] The second flight took place on October 7, 1981; both flights from Holloman AFB, N.M. For the second flight, the interferometer was equipped with a Ge:Cu detector and a spectral filter which cut off the radiation below 550 cm^{-1}. The present report describes salient features of the second flight and results obtained during this flight.

Description of Balloon Flight

The balloon reached a maximum altitude of approximately 28000 m 5000 seconds after launching, stayed aloft at that altitude for the next 15000 seconds, and descended to the ground with the total flight duration of 22000 seconds. The entire flight was clocked using two different systems. One of these is the time code recorded with the PCM telemetry signal. The time flow agreed well with the timing recorded on flight log of various commands issued during the flight. The other is the time on the three-dimensional record of balloon position and velocity. Between these two clock systems, there exists a substantial discrepancy amounting to more than 2000 seconds at the end of the flight. In this report, describing the

flight, we shall use the time flow which was on the PCM telemetry signal.

The SCRIBE instrumentation was described previously in detail.[1,3] We shall discuss presently only those areas particular to the second flight. The entire scheme pertinent to the flight phase is shown in the diagram of Figure 1. The interferometer, housed in a cryogenic chamber, operated satisfactorily at 77°K for the entire 22000 seconds of flight. The laser beam was provided to the interferometer circuit through an optical fibre (as was done for the 1980 flight) from the laser unit mounted external to the cryogenic chamber. Again for some unknown reason, the laser reference fringes were lost during some portion of the flight, resulting in the loss of the interferogram data. The first such data loss occurred approximately 1200 seconds after launch when the balloon had reached an altitude of approximately 10,000 m. The laser signal was recovered at 11,000 seconds. After several intermittent disappearances, the laser signal was finally stabilized at 14,000 seconds up to 19,000 seconds when the data-taking was terminated. When the laser signal became faulty, the interferogram data were sampled with erroneous sampling intervals; no satisfactory spectral recovery being possible for those interferogram data.

The telemetry radio link worked satisfactorily during the entire flight. No difficulties were encountered in obtaining synchronization of the PCM signal for extracting the data for the decoding operation.

The interferometer's line of sight was controlled using motor drives external to the cryogenic chamber. A front mirror assembly can be made to intercept the line of sight of the interferometer; another unit controls

the elevation angle of the complete interferometer package. Both devices were activated by command signals issued from the ground. In addition to the 45-degree mirror, a blackbody source at ambient temperature can be moved into the field of view of the interferometer for calibration purposes. When the 45-degree mirror was in position, the line of sight of the interferometer was directed downward at an angle of 90 degrees from the optical axis of the interferometer. By commands from the ground it was possible to view either the blackbody or the ground; the latter case occurring when the 45-degree mirror was in position. The other drive unit was used to tilt the entire interferometer package so that atmospheric emission could be observed along various elevation angles, ranging from +7.5° to -5.9° from the horizontal; with the 45-degree mirror out of the FOV.

The control commands issued to the balloon gondola from the ground during the flight are listed chronologically, with various other information, in Table I. A schematic diagram summarizing the data measurement during the entire flight is shown in Figure 2.

Processing of Data

The recorded telemetry data were processed at UMass. A detailed description of the post-flight processing may be found in previous reports.[4,5] A schematic diagram of the processing scheme is shown in Figure 3. Approximately 180 useful spectra were recovered with a resolution of 0.2 cm^{-1}. More data for the blackbody calibration spectra could be obtained if necessary, however, no attempt was made to recover more of the latter since these would be redundant. The rather low value of S/N of the data

prevented our extending the interferogram data processing beyond the resolution figure of 0.2 cm^{-1}. In Table II the entire recovered spectral data are summarized. There is some ambiguity in correlating the balloon altitude to the spectral data recovered because of a discrepancy between the two time codes.

Results

Typical spectra obtained during the flight are shown in Figures 4 through 27, together with the corresponding first 1000 interferogram data points. The detector amplifier had automatic gain control for recording the interferogram data with appropriate magnitudes.[3] The gain setting of each recovered interferogram data was estimated from the noise level in the recorded interferogram. The observed total radiance level was then computed from the interferogram modulation at the region of central maximum. Strictly speaking the total radiance level estimated in the above procedure would become meaningless if the spectral pattern of radiation were not constant. For the spectral data obtained at the balloon peak altitude this spectral structure remained unchanged, even though the intensity integrated over the spectral range varied considerably. Therefore we feel our estimate is reasonably accurate. The observed radiance level is listed in Table II with identification of the recovered spectra. Figure 28 shows the observed total radiance level plotted as a function of flight time, together with the estimated balloon altitude. Even though the radiance level varied in correlation with the balloon altitude, the amount of its variation far exceeded the total observed

molecular column density estimated for the specific balloon altitude.

At present, calibration of the observed spectra is still incomplete. There are two problems involved in the calibration of the spectra: (1) The temperature information of the blackbody calibration source is not known to good accuracy because the recording system for the blackbody temperature failed after 17:00 GMT. At the time of failure, the recorded temperature for the blackbody calibration source was 259°K, which was considerably higher than ambient. (2) The spectra for the blackbody calibration suggested a blackbody radiation temperature for the source much closer to the ground temperature observed in the down-looking spectra. In contrast to this observation, the source was expected to have a temperature very close to ambient (see Figure 29). At present, we have no way of resolving this uncertainty. We finally decided to adopt a temperature of 270°K for the blackbody source. The relative spectral sensitivity of our instrument was derived based on the 270°K calibration source temperature as shown in the curve of Figure 30.

The obtained spectra shown in Figures 11, 13, 23, 25, and 27 are scaled with the radiance level determined using the above calibration procedure. [Note: The ordinate scales should be read for the value at 700 cm^{-1}, since the spectral plots are not corrected for the relative spectral sensitivity of instrument. The data are, therefore, distorted.]

Conclusion

The two spectra, the vertical and horizontal looking, with expanded wavenumber scale are shown in Figure 31 from 600 cm^{-1} to 800 cm^{-1}. These

show the observed spectral structure in detail. The major CO_2 bands involved in the observed transitions are schematically shown in Figure 32. The theoretically estimated emission spectrum calculated for the horizontal path using the AFGL FASCODB and the AFGL atmospheric line parameter listing is shown in Figure 33. The various parameters for the computation are listed in the figure caption.

The vertical [down]-looking spectral data are found to agree reasonably well with the theoretical estimate, not only in spectral structural appearance but also in radiance level.

In the past no spectrometry (with reasonably high resolution) was attempted of the atmospheric infrared emission along a horizontal path. With a spectral resolution of 0.2 cm^{-1}, which is fine enough to resolve most of the line structure, our data provided remarkable information on the atmosphere at altitudes of 27000 ~ 28000 m. There were two distinctive features to be observed from our data.

The first feature is the existence of a continuum background superimposed on the molecular [line] structure. At the balloon peak altitude of 28,500 m, the data contain a continuum level amounting to more than 50% of the molecular feature. This feature was found throughout the data obtained at high altitude, 27,500 ~ 28,500 m. We have no idea what caused this continuum background radiance level. The interferometer's line of sight was locked at the elevation angle of +7.5°. There is a very remote possibility that the emission from a thick lower layer atmosphere was being observed. If we were to observe the emission from the ZnSe window or something inside the interferometer compartment, the radiance level would

have remained constant, independent of the input radiance level. The instrumentally originated radiation, thus, cannot enter into our consideration because the radiance amount in question varied with the total radiance level contained in the input signal. The continuum radiation in question was strongly correlated with the atmospheric emission observed. This phenomenon must be looked into more thoroughly in the future.

The second finding, very interesting to us at present, is the varying amount of observed radiance level. From the spectral data in Q to those in T of Table II, the radiance level increased by approximately 50%, while the balloon altitude remained at the same altitude of 28,500 m. Contrary to the observed atmospheric radiance level, the radiance level of calibration spectra remained constant from those of L to those of 2 and 3. Toward the end of the flight, the balloon descended to 27,500 m when the spectral data of 4 through 6 of Table II were taken. The radiance level meanwhile increased to a level at least four times that observed at the maximum altitude. Again, we recall that there was some discrepancy between the PCM time code and that used in the record of balloon location. Even with this discrepancy accounted for, the balloon altitude was found to be well above 27000 m. It is rather mysterious that the radiance level of spectral data changed so much with little change in spectral structure. It is unclear to us whether these facts suggest the stratosphere is rather violently disturbed, or whether the detector sensitivity varied considerably during the flight. The blackbody radiation calibration spectra, however, strongly suggest that the detector sensitivity remained constant. At present, we cannot resolve the two observations dominant in our data and these problems will be addressed in future work.

Acknowledgment

Many individuals made their contribution to the work reported here, even though they are not involved in the actual writing of this report. J. Pritchard of Idealab, Inc., designed and fabricated the interferometer. F.J. Murcray and F.H. Murcray of the University of Denver made the entire balloon instrumentation airworthy and participated in the balloon flight. T.C. Li, W. Barowy, S. Pulchtopek, and L. Barron of the University of Massachusetts participated in the post-flight data processing. A. Gianetti of AFGL directed the balloon flight. W. Gallery of AFGL provided the synthetic spectrum calculated using the FASCODB. We express our appreciation for their efforts.

References

1. G. Vanasse, "Stratospheric Cryogenic Interferometer Balloon Experiment," AFGL Report (1981).
2. H. Sakai *et al.*, "Measurement of Atmospheric Emission Using A Balloon-Borne Cryogenic Fourier Spectrometer," Proc. 1981 Int'l Conf. on Fourier Transform Infrared Spectroscopy, p. 196 (1981).
3. U. Denver, Final Report, F19628-78-C-0164.
4. H. Sakai, U. Mass., Scientific Report AFGL-TR-81-0129.
5. H. Sakai, U. Mass., Final Report AFGL-TR-82-0055.
6. F. Murcray, Jr., communication to H. Sakai.

SCRIBE II Flight History

Table I

GMT	
14:26	Launch
14:46	Bias up
	Loss of laser fringe modulation
14:56	Elevation angle changed to 4.6°
15:04	Elevation angle changed to 1.1°
15:20	Elevation angle changed to -0.8°
16:07	Auxiliary power--off
16:09	*Blackbody inserted in FOV*
16:10	Mirror stepped to downward looking
	Auxiliary power--on
16:25	Fine ballast power
16:27	Bias down
16:41	Latch gas valve open
17:04	Elevation angle changed to -3.4°
	Mirror stepped out to clear field
17:09	Bias up
17:10	Auxiliary power--on
	Bias up
17:13	Elevation angle changed to -5.9°
17:25	Unlatch gas valve
17:26	Blackbody inserted in FOV
	Elevation angle restored to 7.5°
17:35	Laser fringe modulation restored; start of the interferogram data recovery

Table I (continued)

GMT	
17:36	Mirror stepped out to clear field
17:36 to 17:42	Horizontal path interferogram data at $\theta = 7.5°$
17:41	Mirror stepped for the downlooking position
17:44	Loss of laser fringe modulation
	Loss of interferogram data
17:51	Open gas valve
18:05	Latch gas valve open
18:08	Main power--on
18:10	Recovery of laser fringe modulation
	Recovery of interferogram data
18:12	Mirror stepped out to clear field
18:14	End of the downward-looking measurement
18:15	Start of the horizontal path measurement $\theta = 7.5°$
18:23	Main power--on
18:53	Blackbody inserted in FOV
	Beginning of blackbody calibration interferogram data
18:59	Unlatch gas valve
19:00	End of blackbody calibration data recovery
19:25	Mirror stepped out to clear field
19:26	Beginning of the horizontal path data recovery $\theta = 7.5°$
19:32	Auxiliary power--off
19:35	End of the horizontal path data recovery
19:35	Mirror stopped in position
19:40	Bias down

Table I (continued)

GMT	
19:46	Main power--off
20:09	Latch gas valve open
20:17	Unlatch gas valve
20:18	Main power--on
20:41	Flight terminated

Table II

Recovered Spectral Data

GMT	ID	Total Radiance (Relative Scale)	Remarks
14:26:19	BA	14.10	Launch
26:48	BB	14.10	
27:19	BC	13.90	
27:48	BD	13.80	
28:18	BE	13.76	
28:48	BF	13.84	
29:18	CA	12.70	
29:49	CB	12.26	
30:18	CC	11.72	
30:48	CD	11.42	
31:18	CE	10.98	
31:47	CF	10.56	
32:17	DA	9.96	
32:47	DB	9.74	
33:17	DC	9.20	
33:47	DD	9.20	
34:17	DE	9.10	
34:47	DF	8.60	
35:17	EA	8.36	
35:46	EB	8.16	
36:16	EC	8.16	
36:46	ED	8.16	
37:15	FA	7.92	
37:45	FB	7.60	

Table II (Continued)

GMT	ID	Total Radiance (Relative Scale)	Remarks
38:15	FC	7.25	
38:45	FD	7.60	
39:15	FE	7.34	
39:45	FF	7.17	
40:15	GA	7.00	
40:51	GB	7.00	
41:20	GC	6.75	
41:52	GD	6.50	
42:22	GE	6.50	
42:52	GF	6.50	
43:51	HA	6.00	
44:21	HB	6.00	
44:52	HC	6.00	
45:21	HD	5.50	
45:51	HE	5.50	
46:21	HF	5.50	After HF, laser signal failed
17:35:57	LB	9.84	Blackbody source calibration
36:27	LC	9.96	" " "
38:57	KA	1.62	Horizontal-looking
39:27	KB	1.65	"
39:57	KC	1.60	"
41:27	MA	1.54	"
41:57	MB	1.54	"
42:27	MC	1.55	"
42:57	MD	--	Down-looking saturated
43:27	ME	--	" "

Table II (Continued)

GMT	ID	Total Radiance (Relative Scale)	Remarks
43:57	MF	8.10	Down-looking
44:57	NA	8.13	"
45:27	NB	8.18	"
45:57	NC	7.91	"
46:27	NO	8.18	"
46:56	NE	7.85	"
47:26	NF	8.25	"
48:26	OA	8.00	"
48:56	OB	8.12	"
49:25	OC	7.90	"
49:55	OD	8.08	"
50:25	OE	8.20	"
50:55	OF	8.18	"
51:25	OG	7.21	"
51:55	PA	--	"
52:25	PB	7.48	"
52:55	PC	7.65	"
53:54	PE	7.20	"
18:13:00	QA	--	"
13:29	QB	7.38	"
13:58	QC	3.52	
14:28	QD	1.62	Front mirror was out
14:57	QE	1.25	Horizontal-looking
15:27	QF	1.15	"
15:57	QG	1.12	"

Table II (Continued)

GMT	ID	Total Radiance (Relative Scale)	Remarks
16:26	RA	1.16	Horizontal-looking
16:56	RB	--	"
17:26	RC	1.18	"
17:56	RD	1.27	"
18:25	RE	1.15	"
18:55	RF	1.15	"
19:24	RG	1.23	"
19:53	SA	1.25	"
20:23	SB	1.18	"
20:53	SC	1.14	"
21:22	SD	1.24	"
26:15	TA	1.69	"
26:45	TB	1.51	"
27:15	TC	1.60	"
27:45	TD	1.64	"
28:14	TE	1.71	"
28:43	TF	1.56	"
30.12	TG	1.07	" , unstable gain setting
30:35	UA	1.08	" " " "
31:05	UB	1.45	"
31:34	UC	1.55	"
32:04	UD	1.52	"
32:33	UE	1.50	"
33:03	UF	1.52	"
33:32	UG	1.44	"
34:02	VA	1.37	"

Table II (Continued)

GMT	ID	Total Radiance (Relative Scale)	Remarks
34:31	VB	1.43	Horizontal-looking
35:00	VC	1.37	"
35:30	VD	1.40	"
35:59	VE	1.45	"
36:28	VF	1.51	"
36:57	VG	1.45	"
37:26	WA	1.50	"
37:56	WB	1.65	"
38:25	WC	1.56	"
38:55	WD	1.57	"
39:24	WE	1.43	"
39:54	WF	1.52	"
40:23	WG	1.52	"
40:53	XA	1.61	"
41:22	XB	1.45	"
41:51	XC	1.47	"
42:21	XD	1.55	"
42:50	XE	1.59	"
43:20	XF	1.50	"
43:49	XG	1.54	"
44:18	YA	1.57	"
44:48	YB	1.57	"
45:17	YC	1.62	"
45:47	YD	1.47	"
46:16	YE	1.57	"
46:45	YF	1.56	"

Table II (Continued)

GMT	ID	Total Radiance (Relative Scale)	Remarks
47:14	YG	1.56	Horizontal-looking
47:44	ZA	1.54	"
48:13	ZB	1.39	"
48:43	ZC	1.69	"
49:12	ZD	1.71	"
49:42	ZE	1.59	"
50:10	1A	1.65	"
50:40	1B	1.58	"
51:09	1C	1.55	"
51:39	1D	1.57	"
52:08	1E	1.48	"
52:38	1F	1.56	"
53:36	2A	1.60	"
54:32	2B	9.90	Blackbody calibration Spectrum
55:04	2C	9.50	" " "
55:33	2D	9.50	" " "
56:03	2E	9.60	" " "
56:32	2F	9.63	" " "
57:02	2G	9.63	" " "
57:31	3A	9.63	" " "
58:01	3B	9.63	" " "
58:30	3C	9.63	" " "
59:28	3E	9.40	" " "
59:58	3F	--	" " "
19:00:27	3G	9.28	

Table II (Continued)

GMT	ID	Total Radiance (Relative Scale)	Remarks
25:50	4A	4.00	Horizontal-looking
26:17	4B	3.92	"
26:46	4C	4.14	"
27:15	4D	4.42	"
27:45	4E	4.62	"
28:14	4F	4.77	"
28:43	4G	5.00	"
29:12	5A	5.17	"
29:42	5B	5.40	"
30:10	5C	5.65	"
30:40	5D	5.90	"
31:09	5E	5.90	"
31:38	5F	5.90	"
32:07	5G	6.09	"
32:30	6A	6.50	"
33:06	6B	6.52	"
33:35	6C	6.74	"
34:04	6D	6.75	"
34:33	6E	6.75	"
35:02	6F	6.80	"
35:31	6G	6.95	"

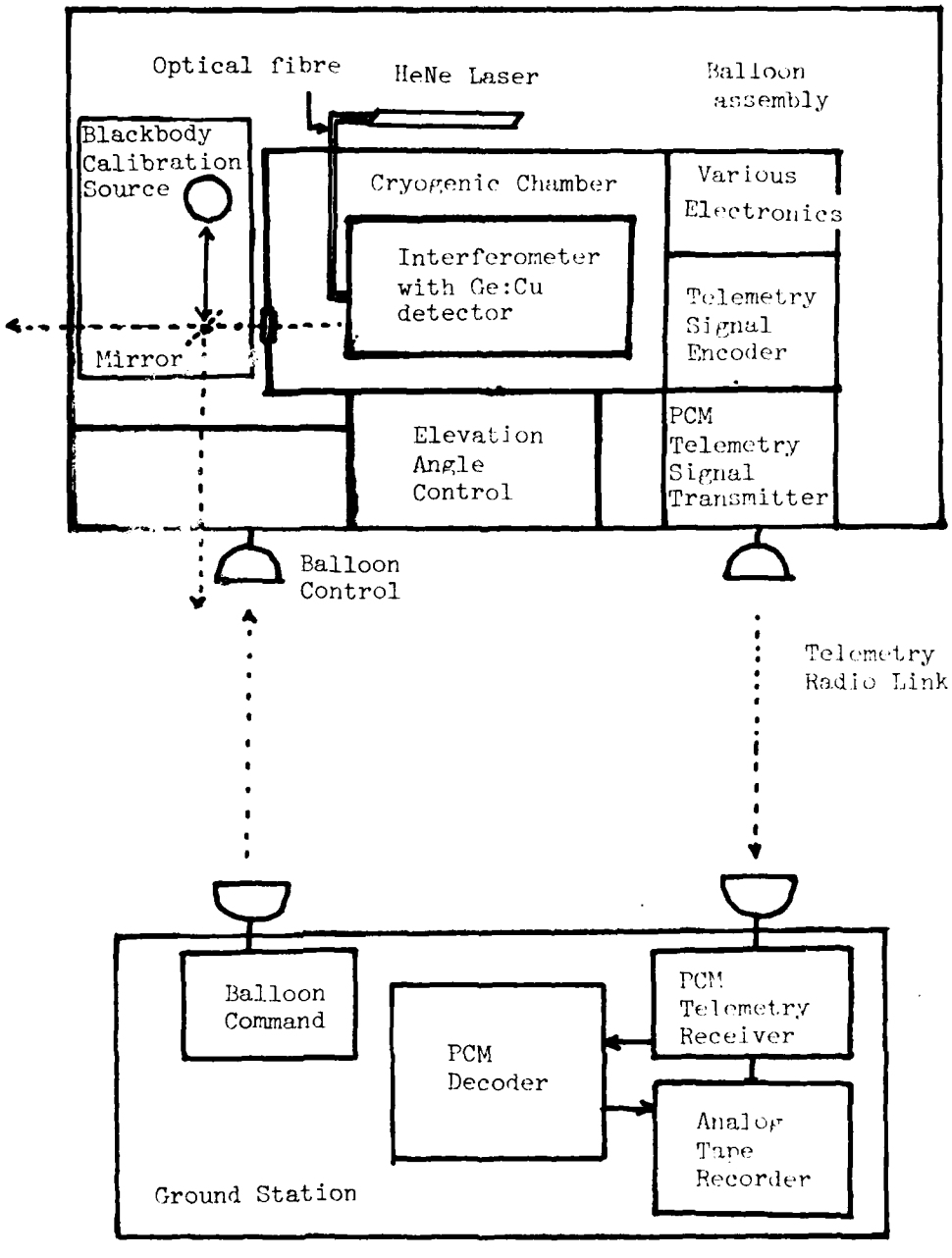

Figure 1

Schematic Diagram of SCRIBE instrumentation.

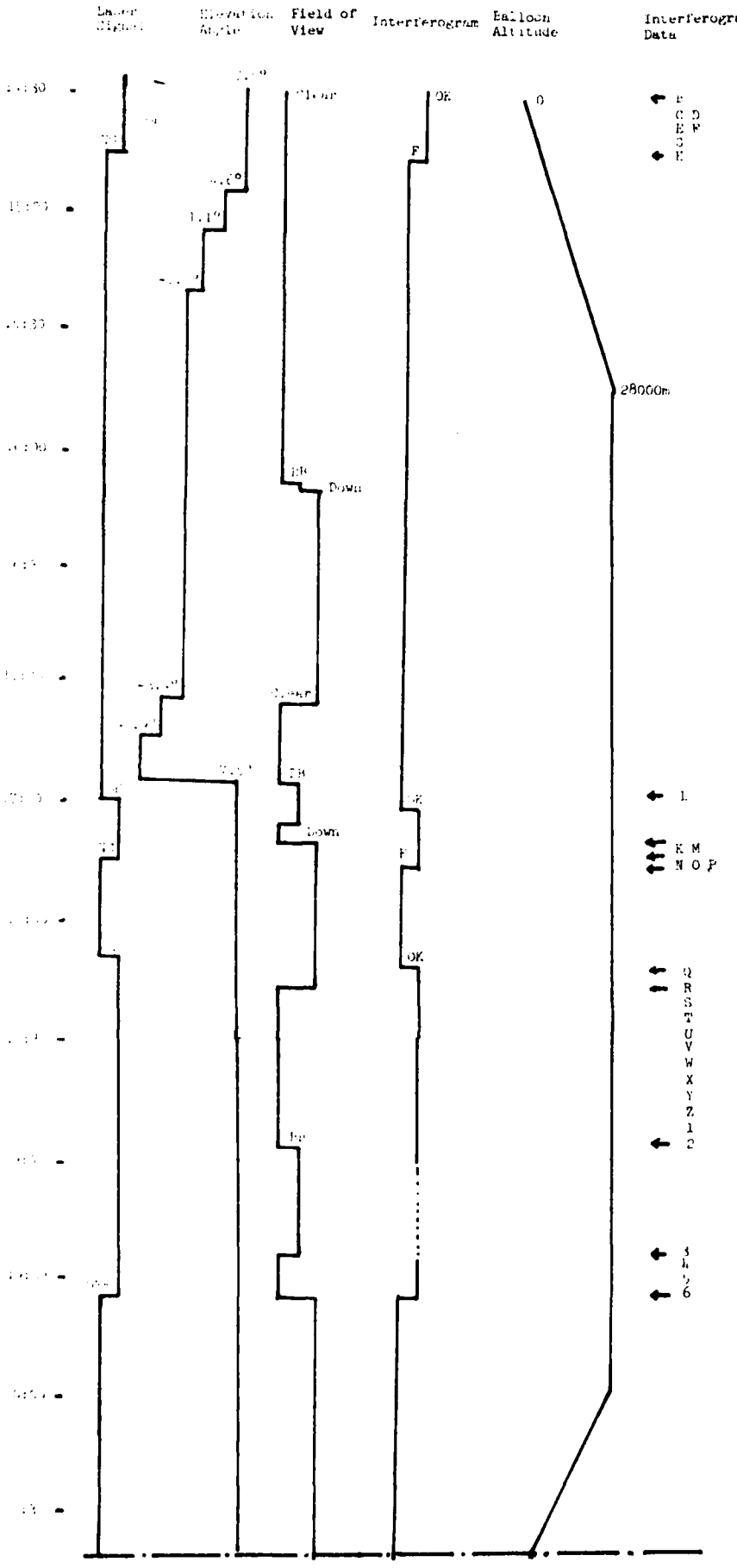

Figure 2

Flight history of SCRIBE II

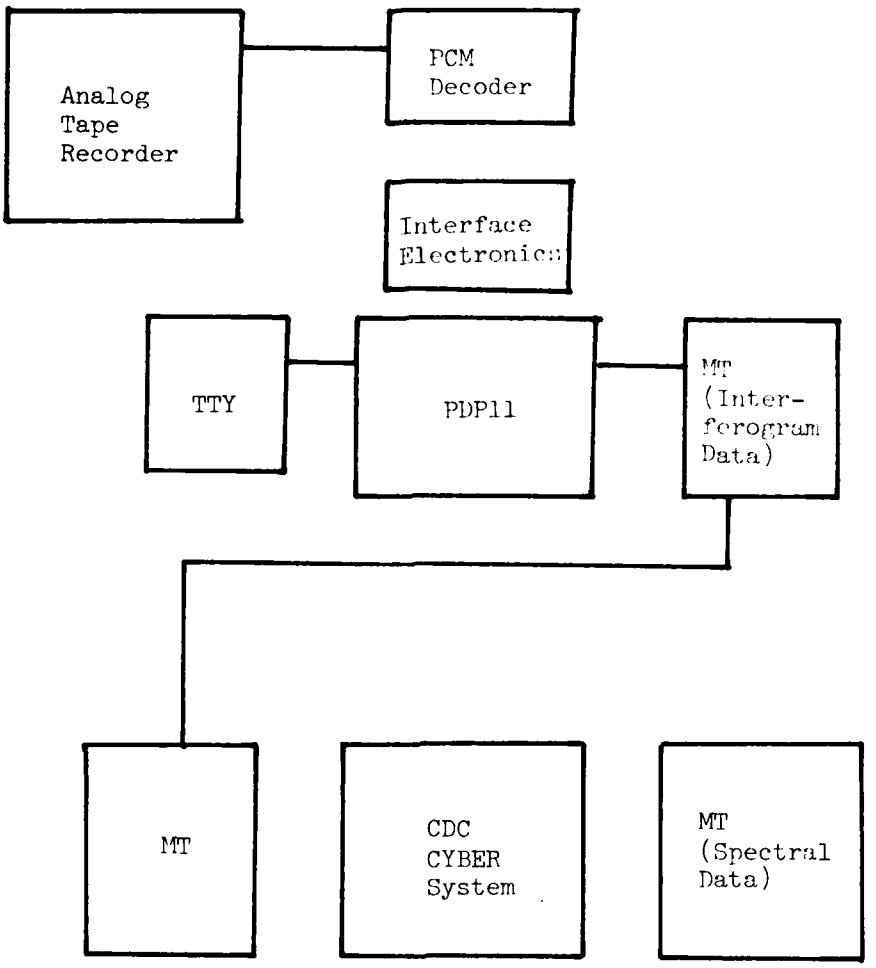

Figure 3

Schematic Diagram of SCRIBE
Post-Flight Processing Scheme

INTDA

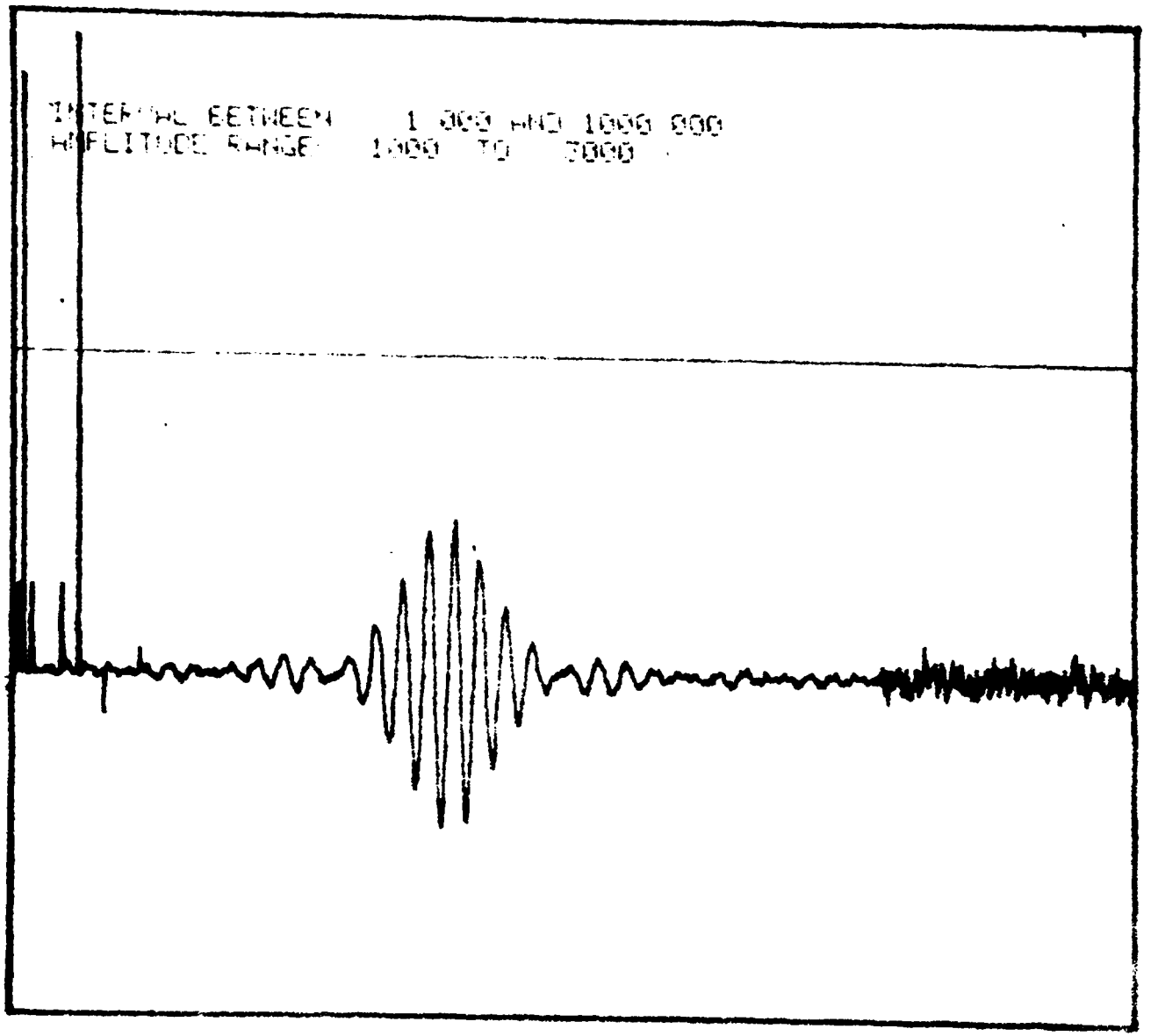

Figure 4

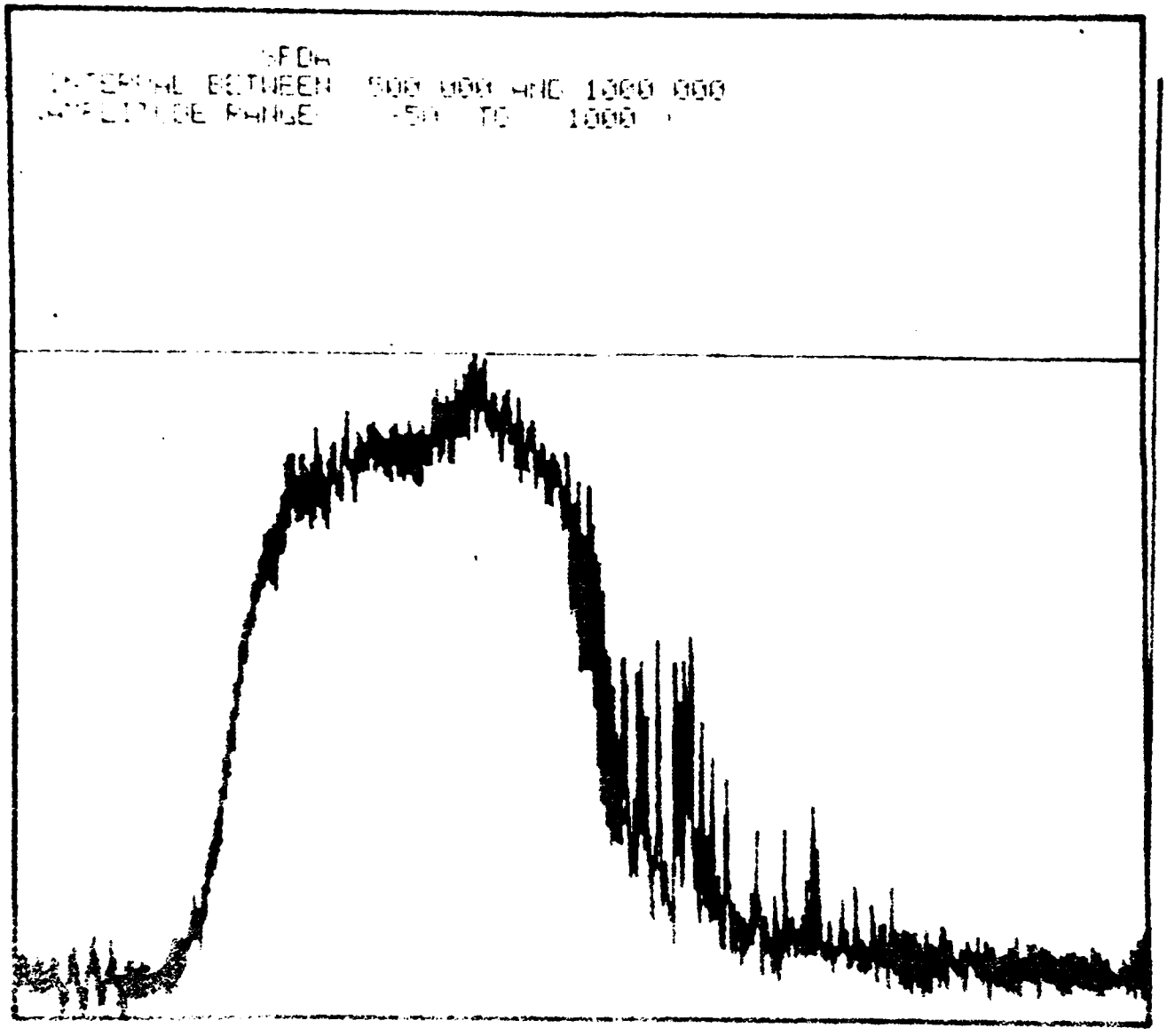
SPDH
INTERVAL BETWEEN 900 000 AND 1000 000
AMPLITUDE RANGE -50 TO 1000

Figure 5

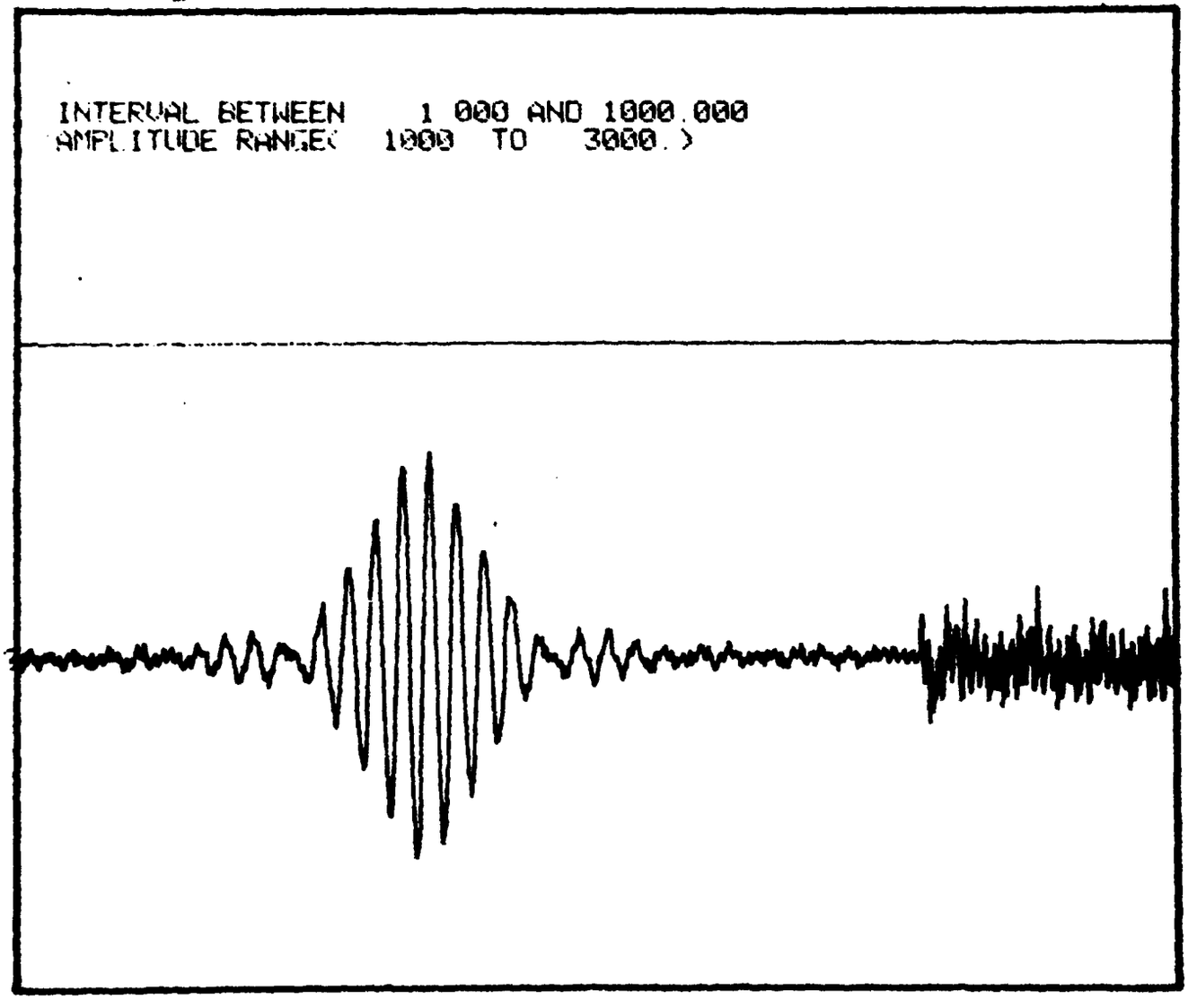
INTERVAL BETWEEN 1.000 AND 1000.000
AMPLITUDE RANGE(1000 TO 3000.)

Figure 6

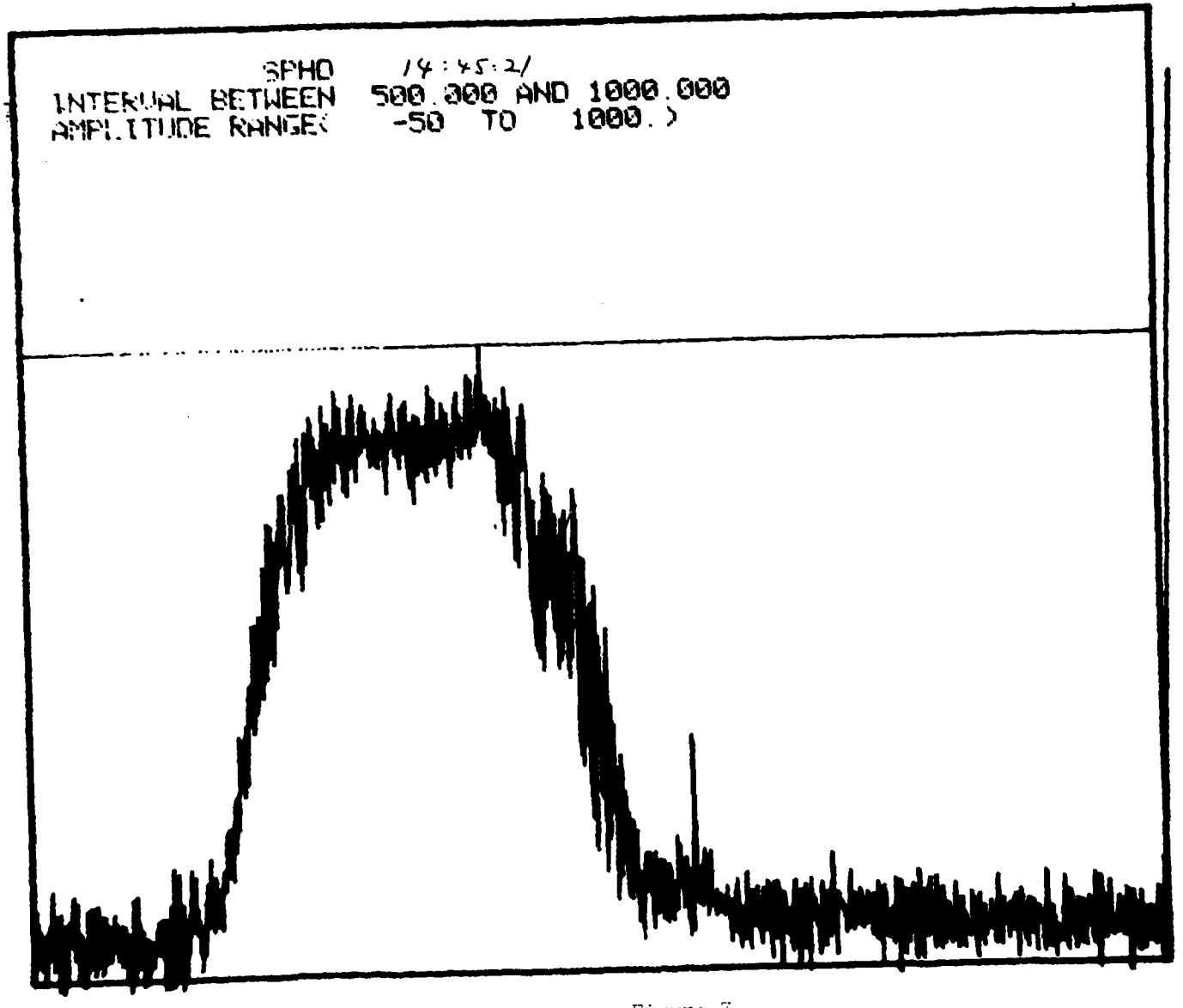
SPHO 14:45:27
INTERVAL BETWEEN 500.000 AND 1000.000
AMPLITUDE RANGE -50 TO 1000.)

Figure 7

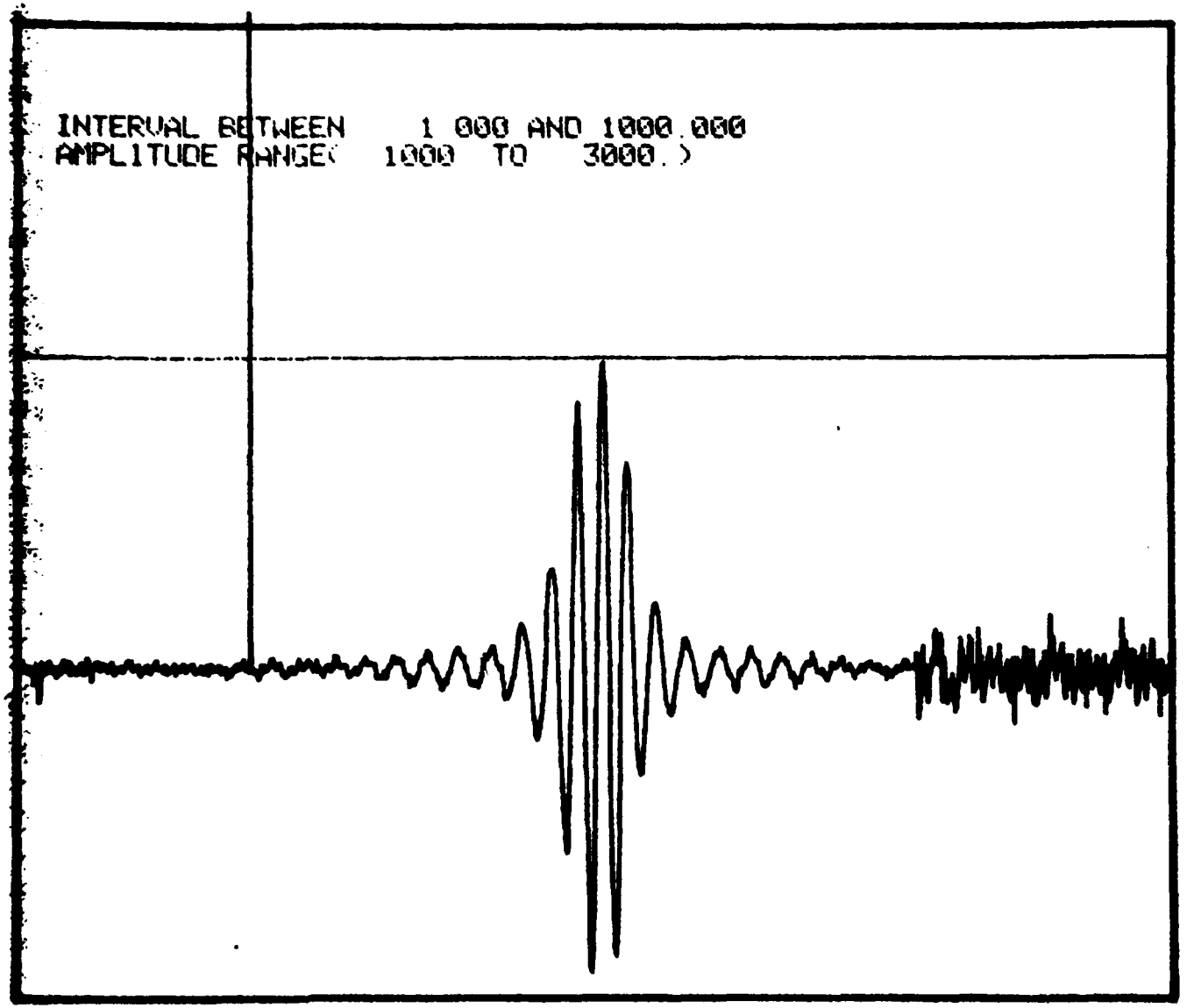
INTERVAL BETWEEN 1 000 AND 1000.000
AMPLITUDE RANGE(1000 TO 3000.)

Figure 8

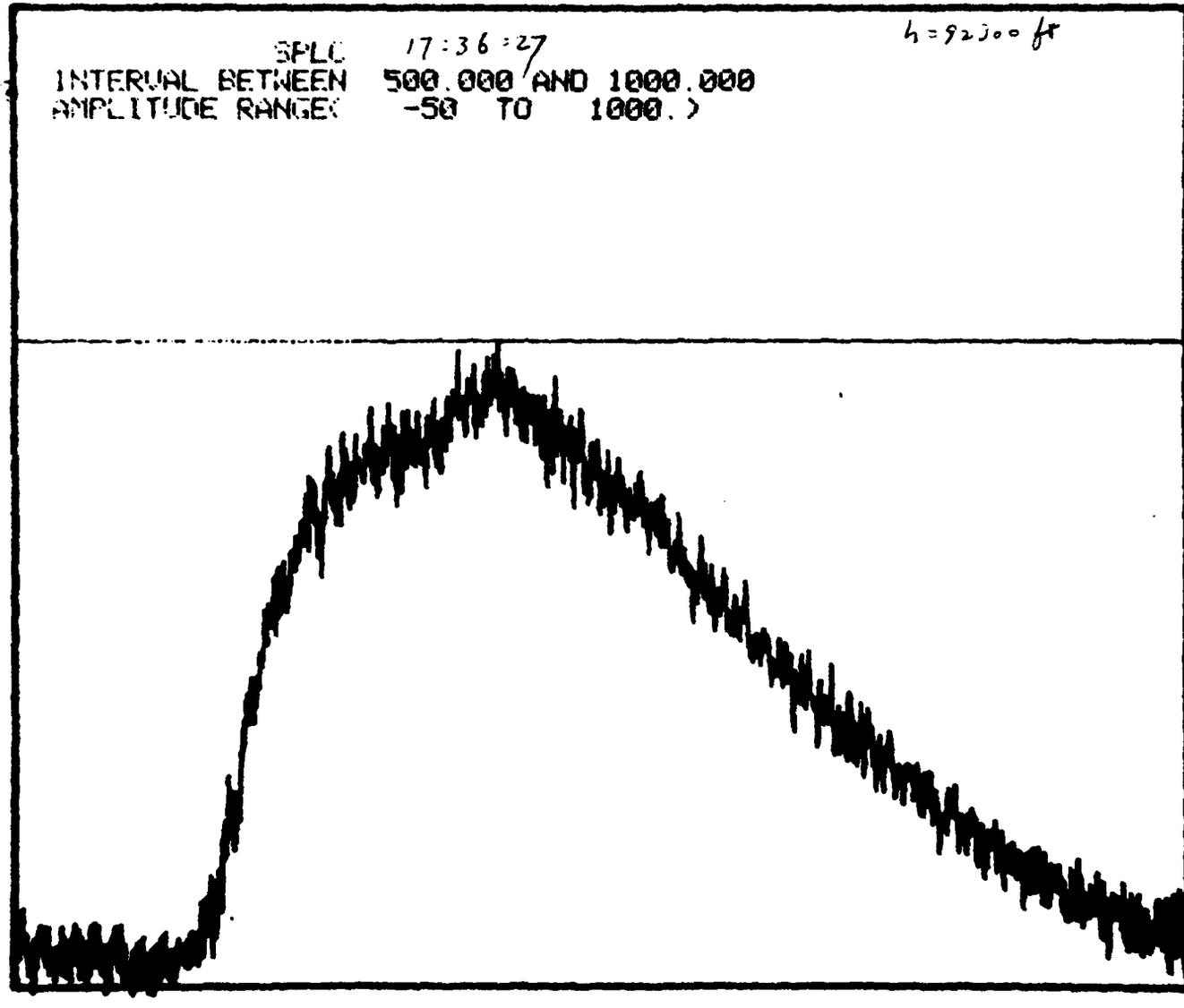
SPLC 17:36:27
INTERVAL BETWEEN 500.000 AND 1000.000
AMPLITUDE RANGE(-50 TO 1000.)
h = 92300 ft

Figure 9

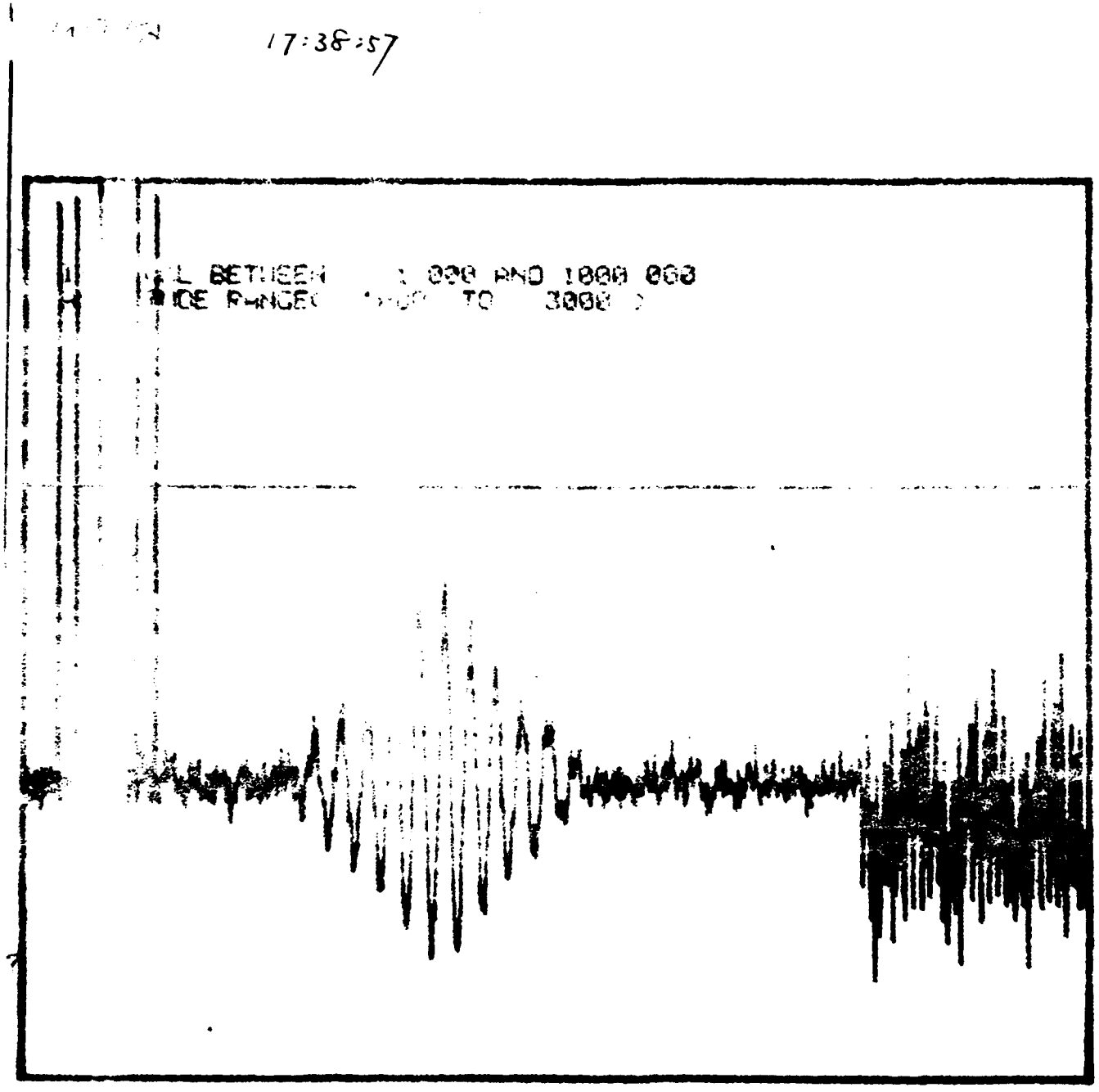

Figure 10

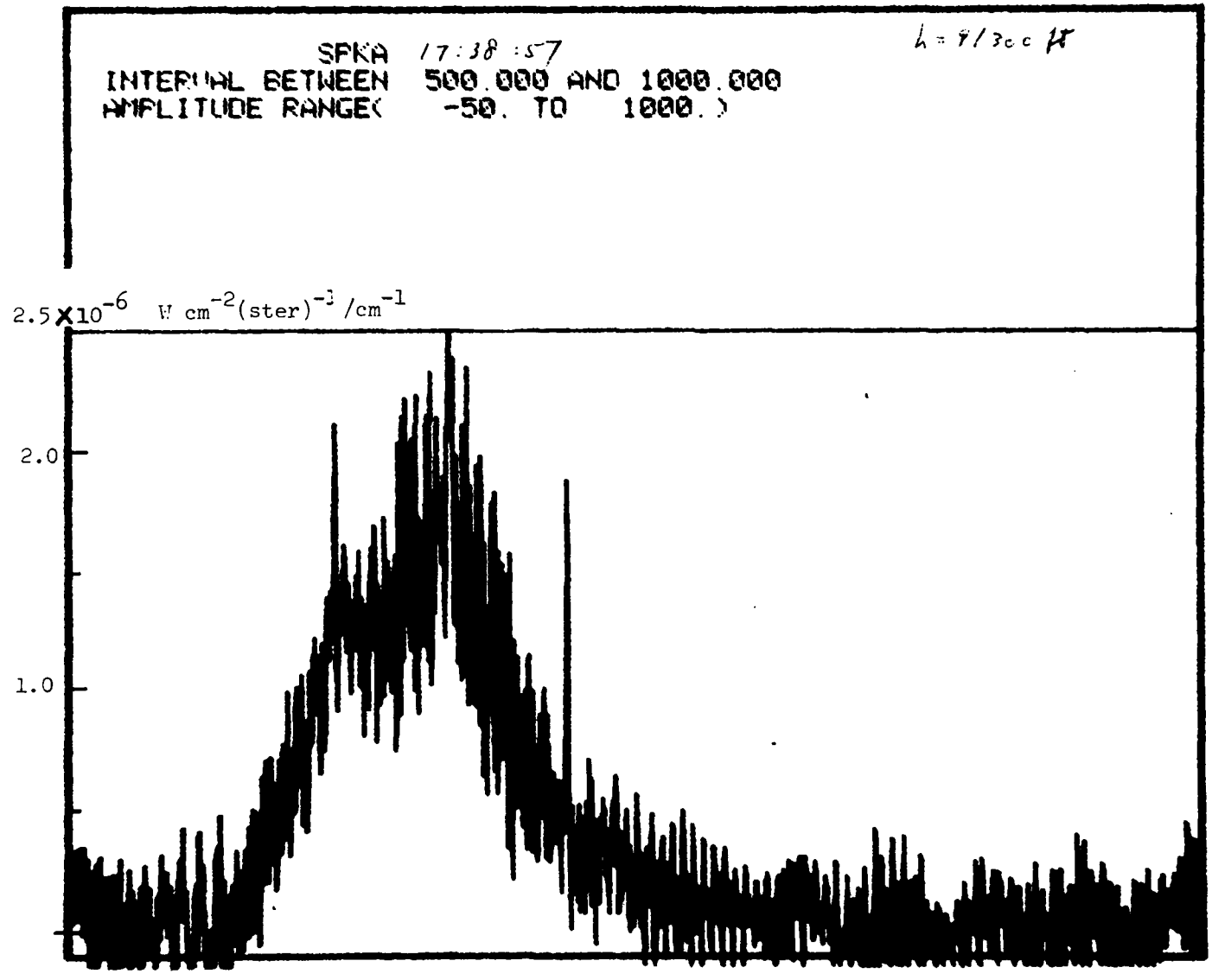
SPKA 17:38:57
INTERVAL BETWEEN 500.000 AND 1000.000
AMPLITUDE RANGE(-50. TO 1000.)
2.5 X10^-6 W cm^-2(ster)^-1 /cm^-1
2.0
1.0

Figure 11

INTMF

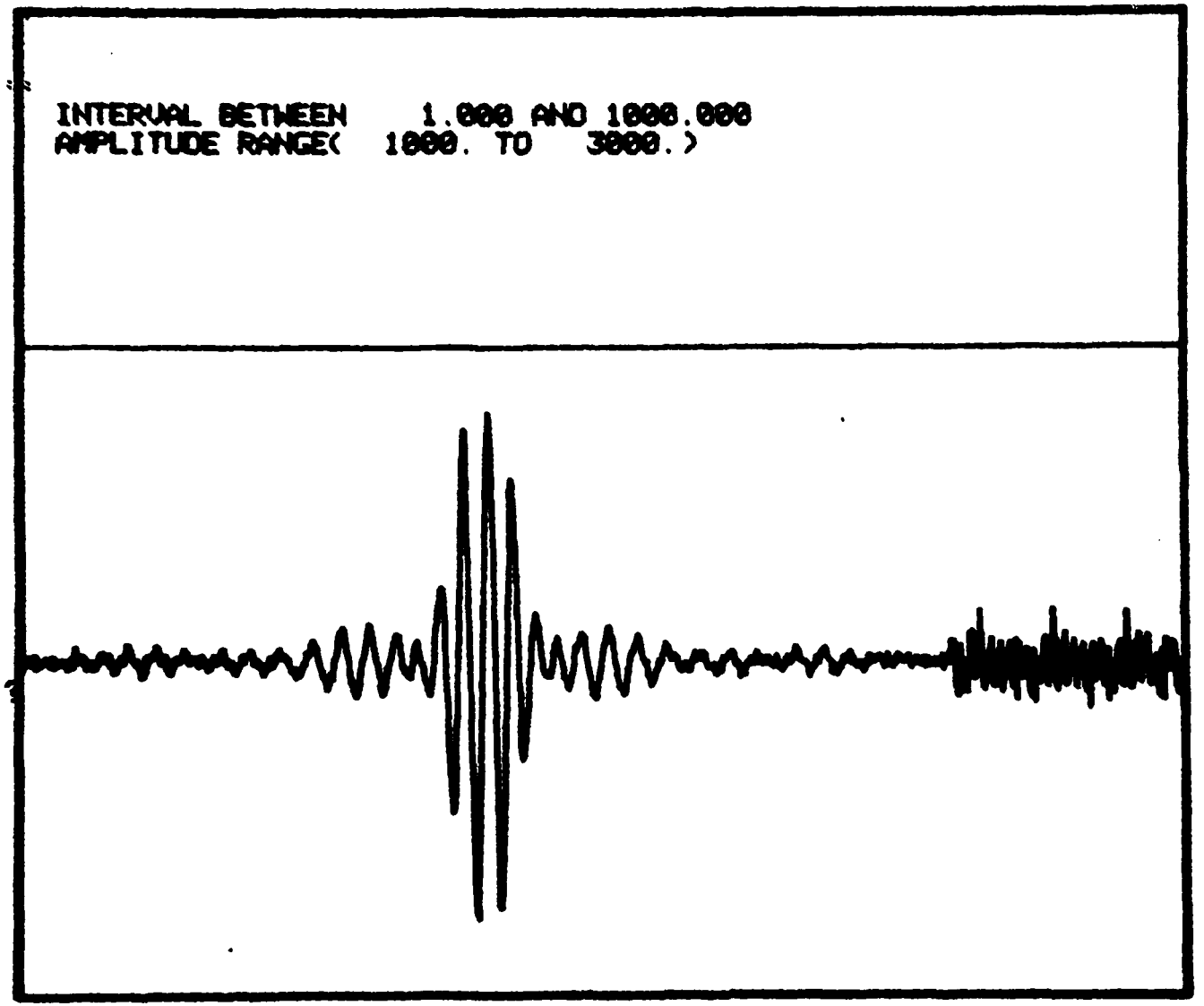

Figure 12

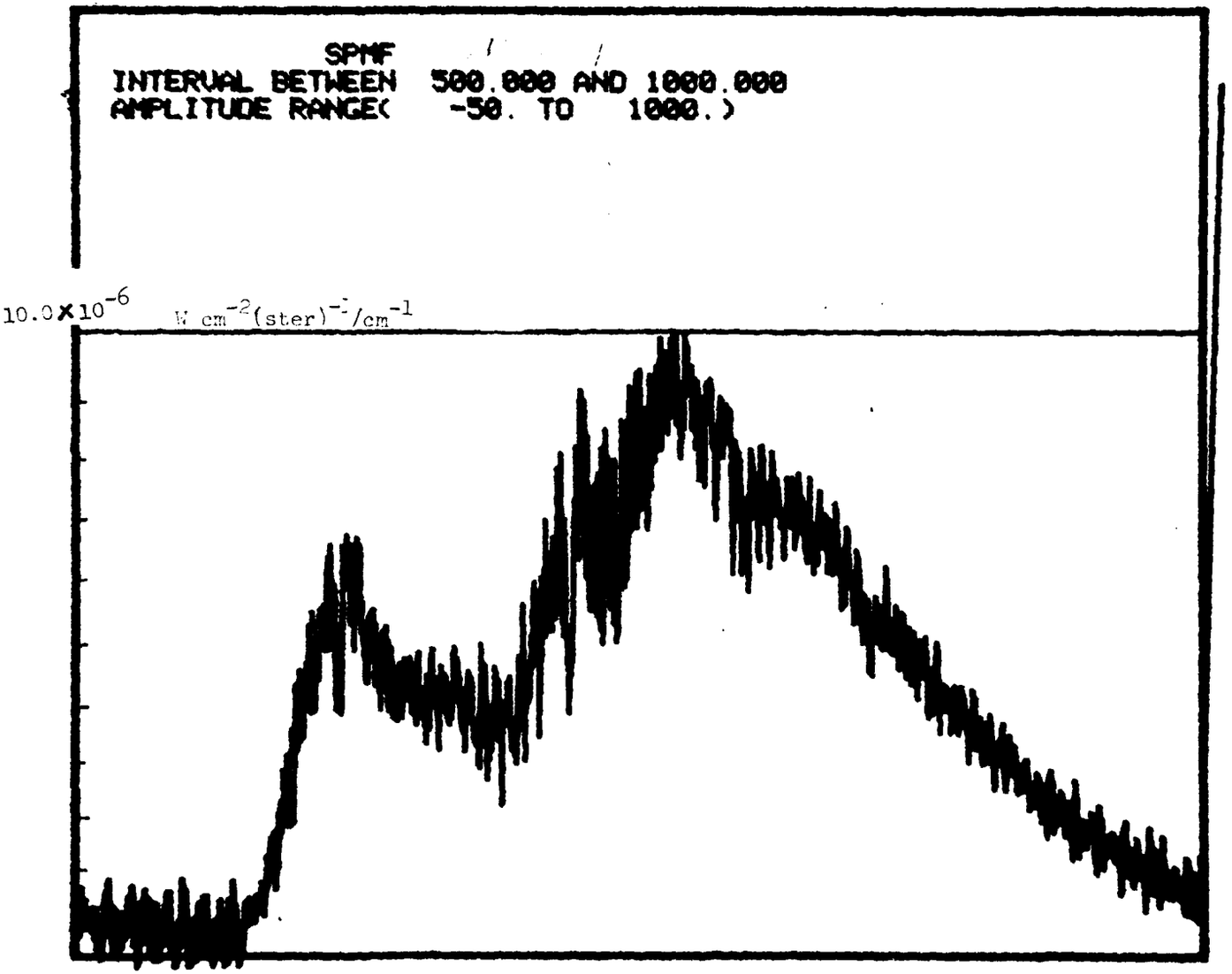
SPMF
INTERVAL BETWEEN 500.000 AND 1000.000
AMPLITUDE RANGE(-50. TO 1000.)
10.0X10-6 W cm-2(ster)-1/cm-1

Figure 1.

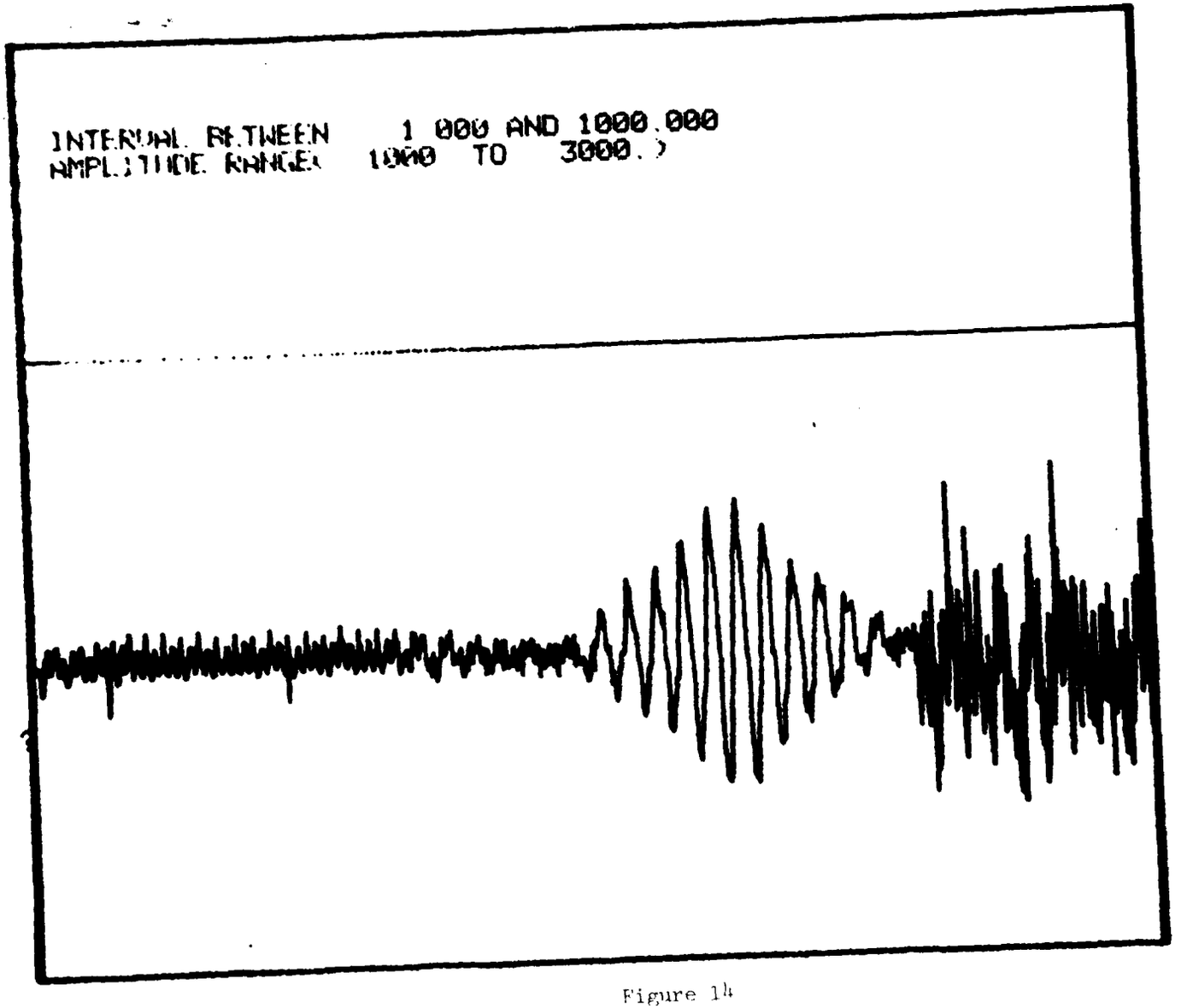
INTERVAL BETWEEN 1 000 AND 1000.000
AMPLITUDE RANGE: 1000 TO 3000.)

Figure 14

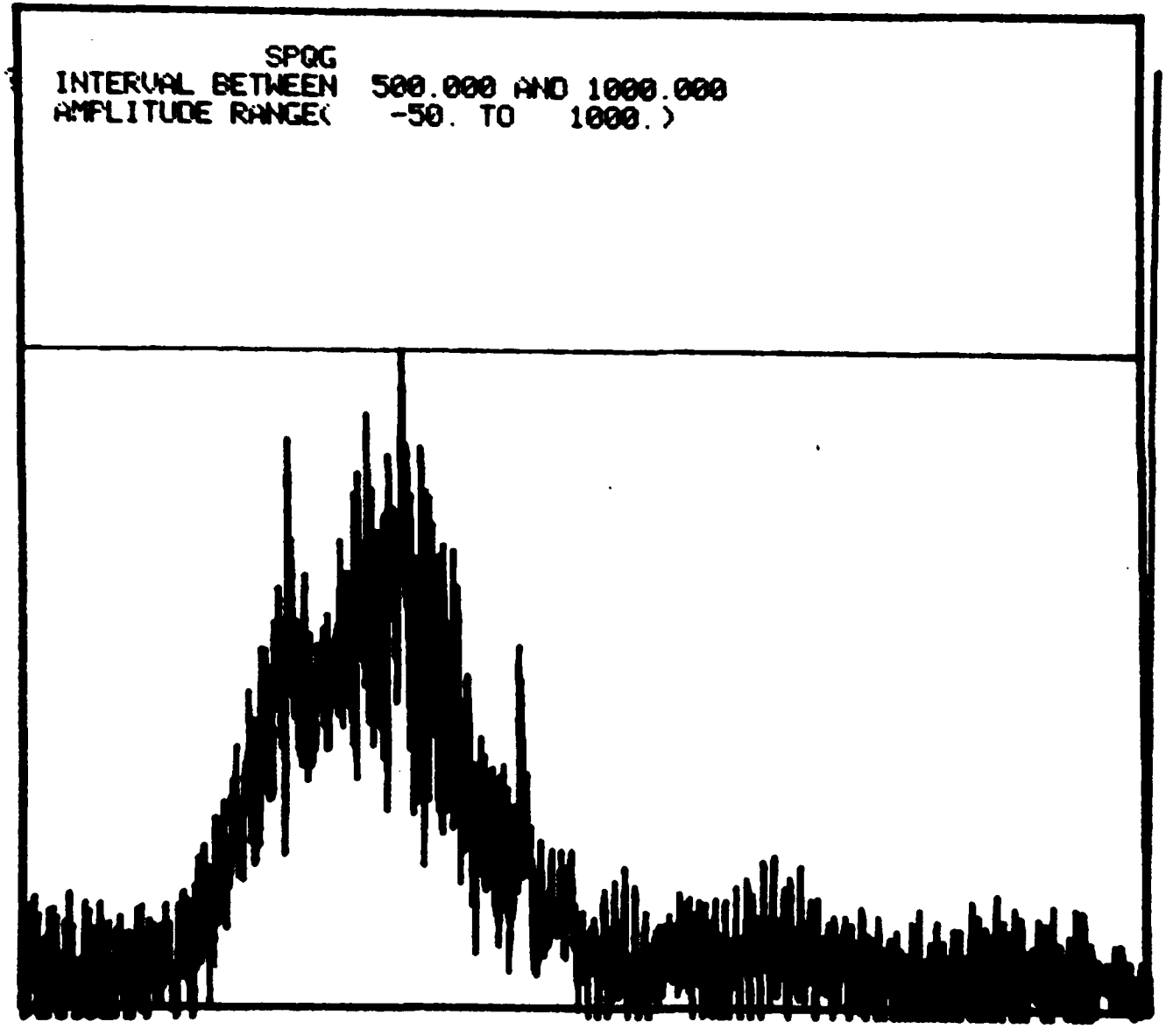
SPQG
INTERVAL BETWEEN 500.000 AND 1000.000
AMPLITUDE RANGE(-50. TO 1000.)

Figure 15

TA

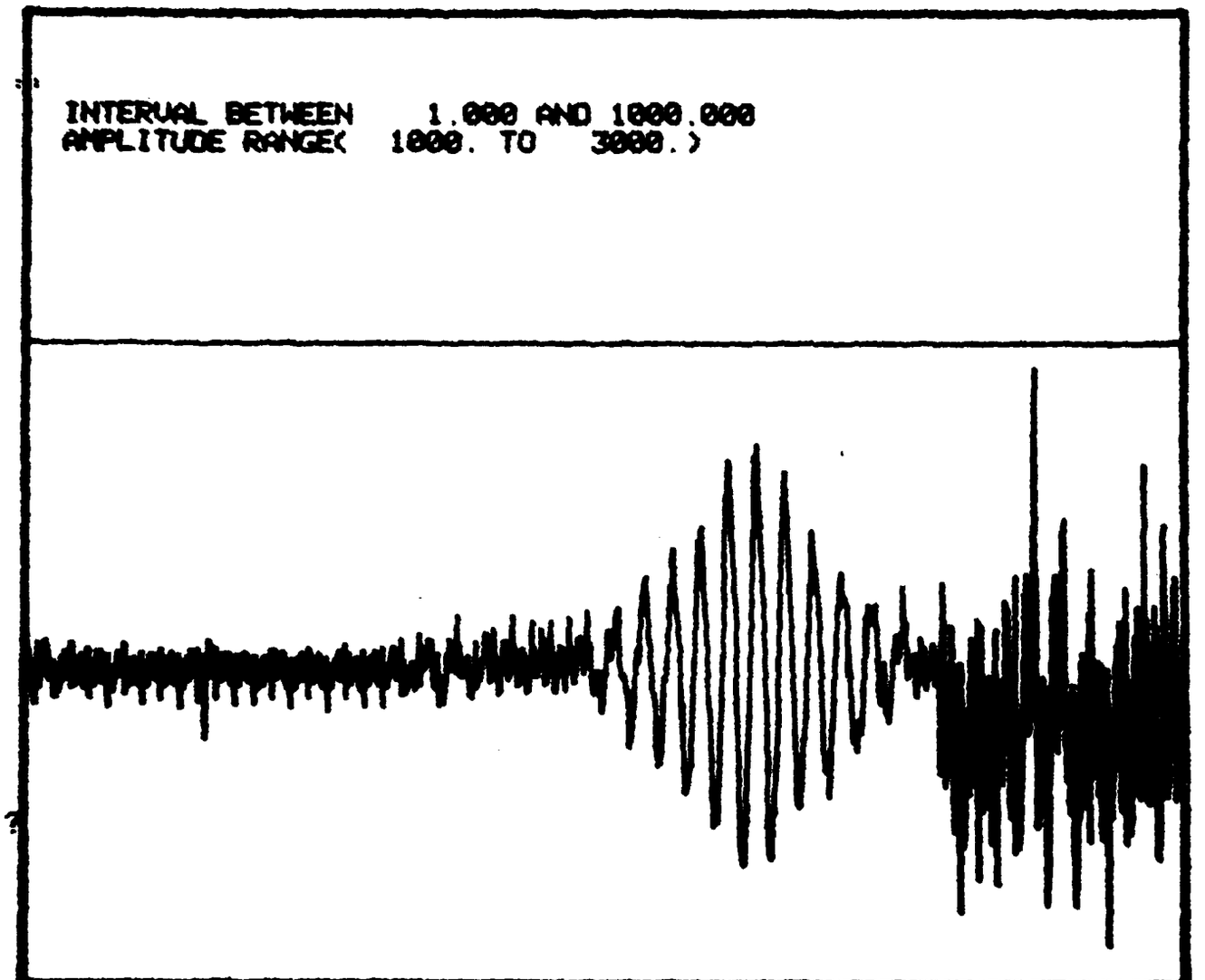
INTERVAL BETWEEN 1.000 AND 1000.000
AMPLITUDE RANGE(1000. TO 3000.)

Figure 16

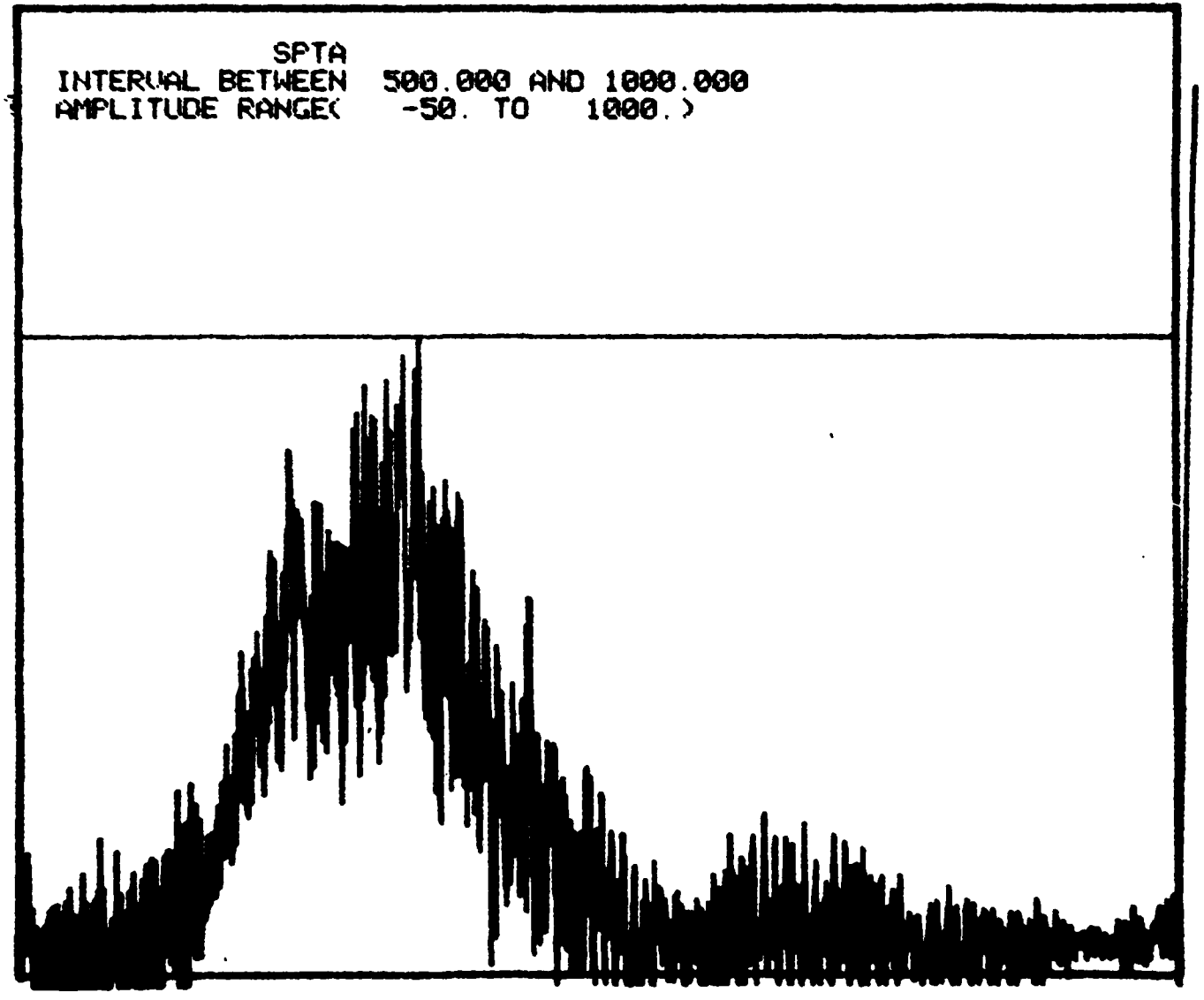
SPTA
INTERVAL BETWEEN 500.000 AND 1000.000
AMPLITUDE RANGE(-50. TO 1000.)

Figure 17

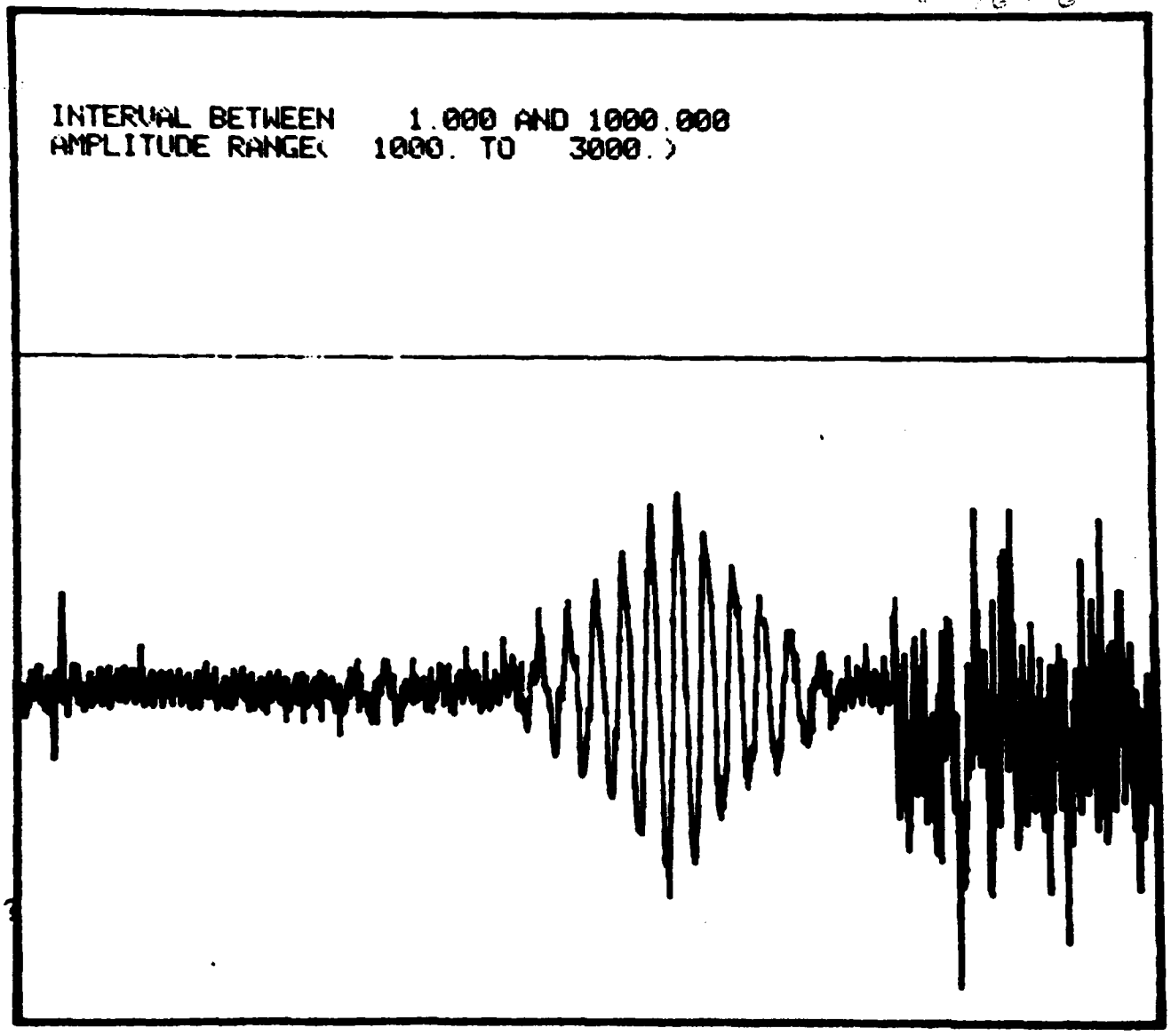
INTERVAL BETWEEN 1.000 AND 1000.000
AMPLITUDE RANGE(1000. TO 3000.)

Figure 18

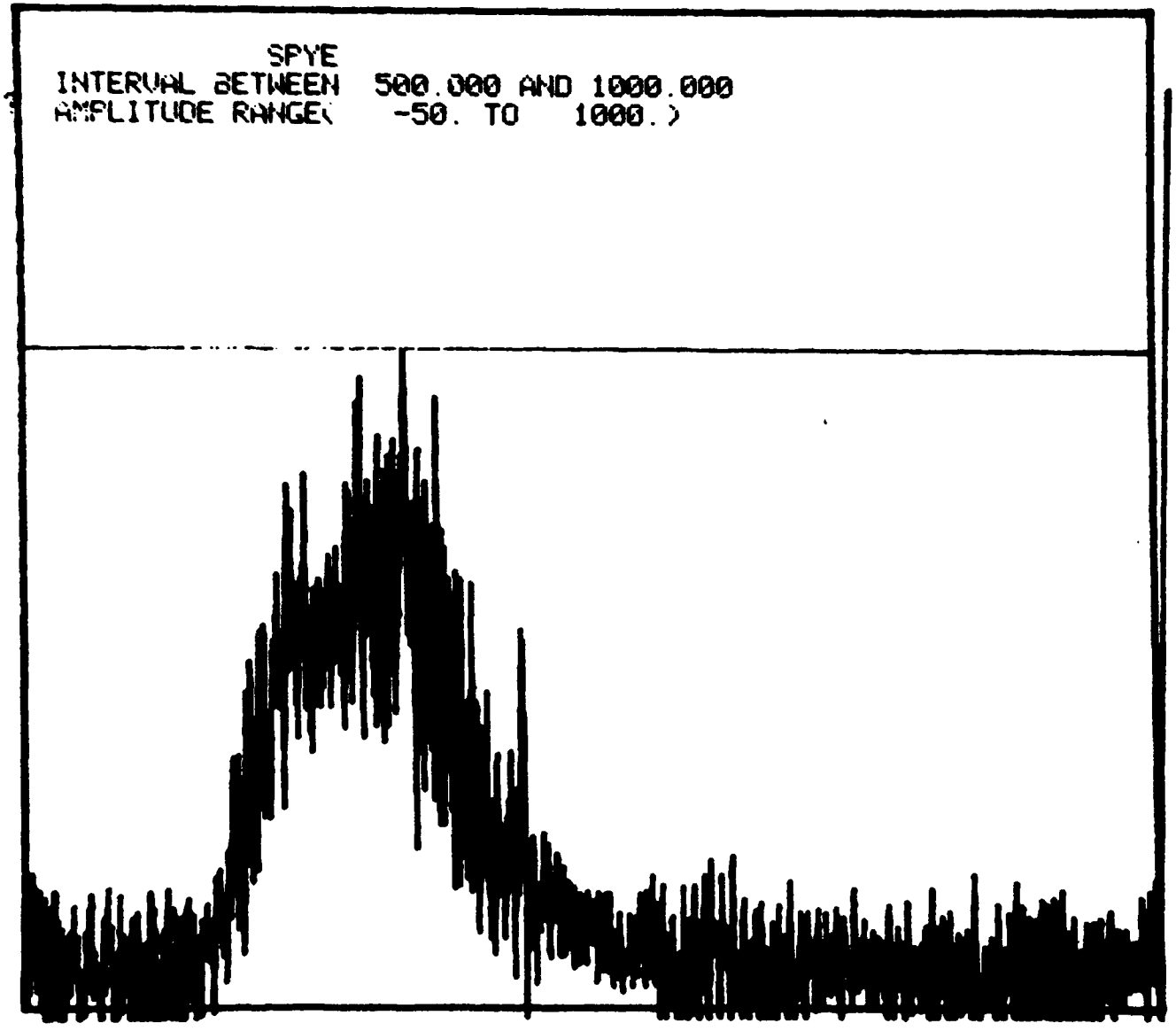
SPYE
INTERVAL BETWEEN 500.000 AND 1000.000
AMPLITUDE RANGE(-50. TO 1000.)

Figure 19

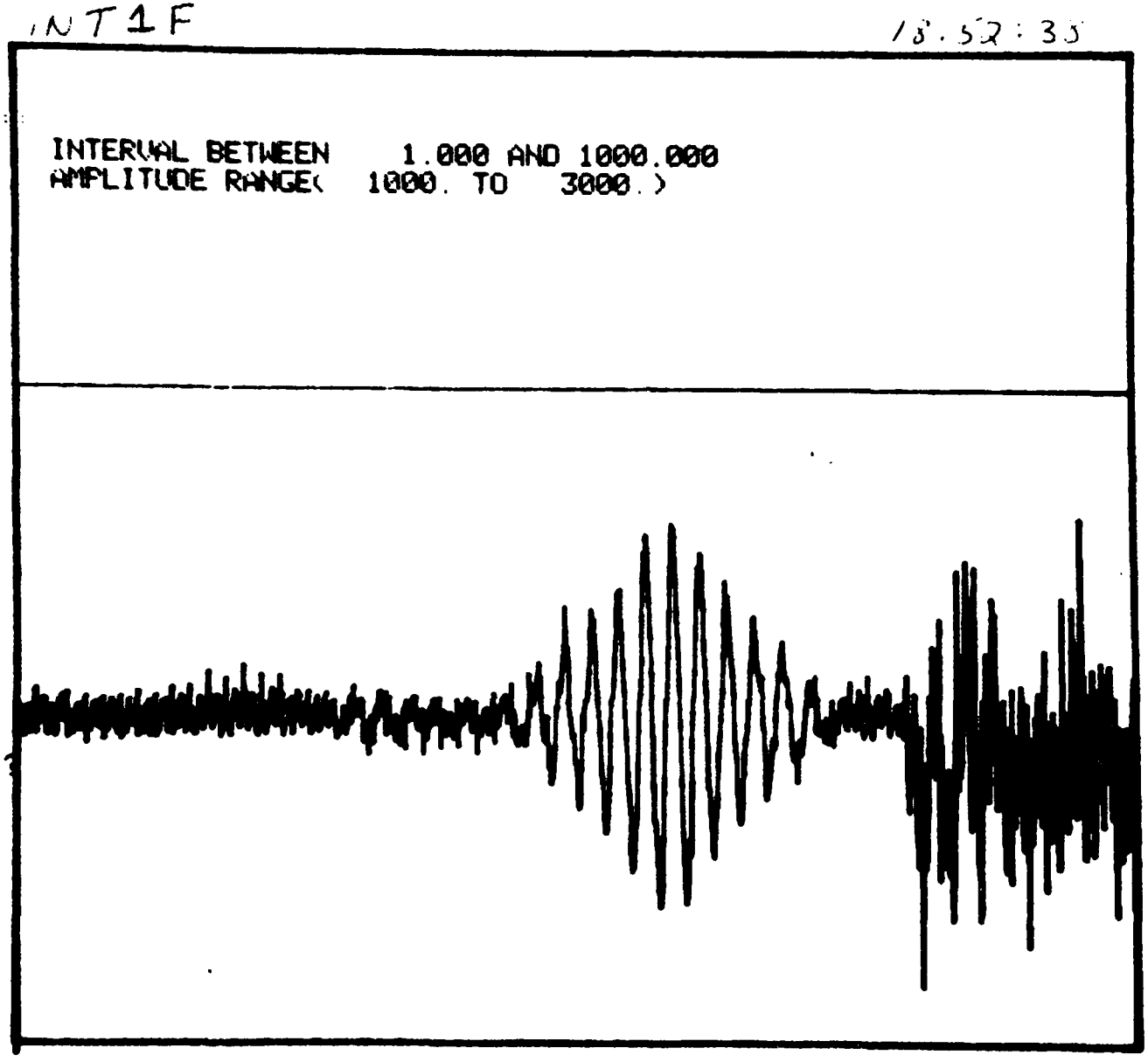
INT1F
18:52:35
INTERVAL BETWEEN 1.000 AND 1000.000
AMPLITUDE RANGE(1000. TO 3000.)

Figure 21

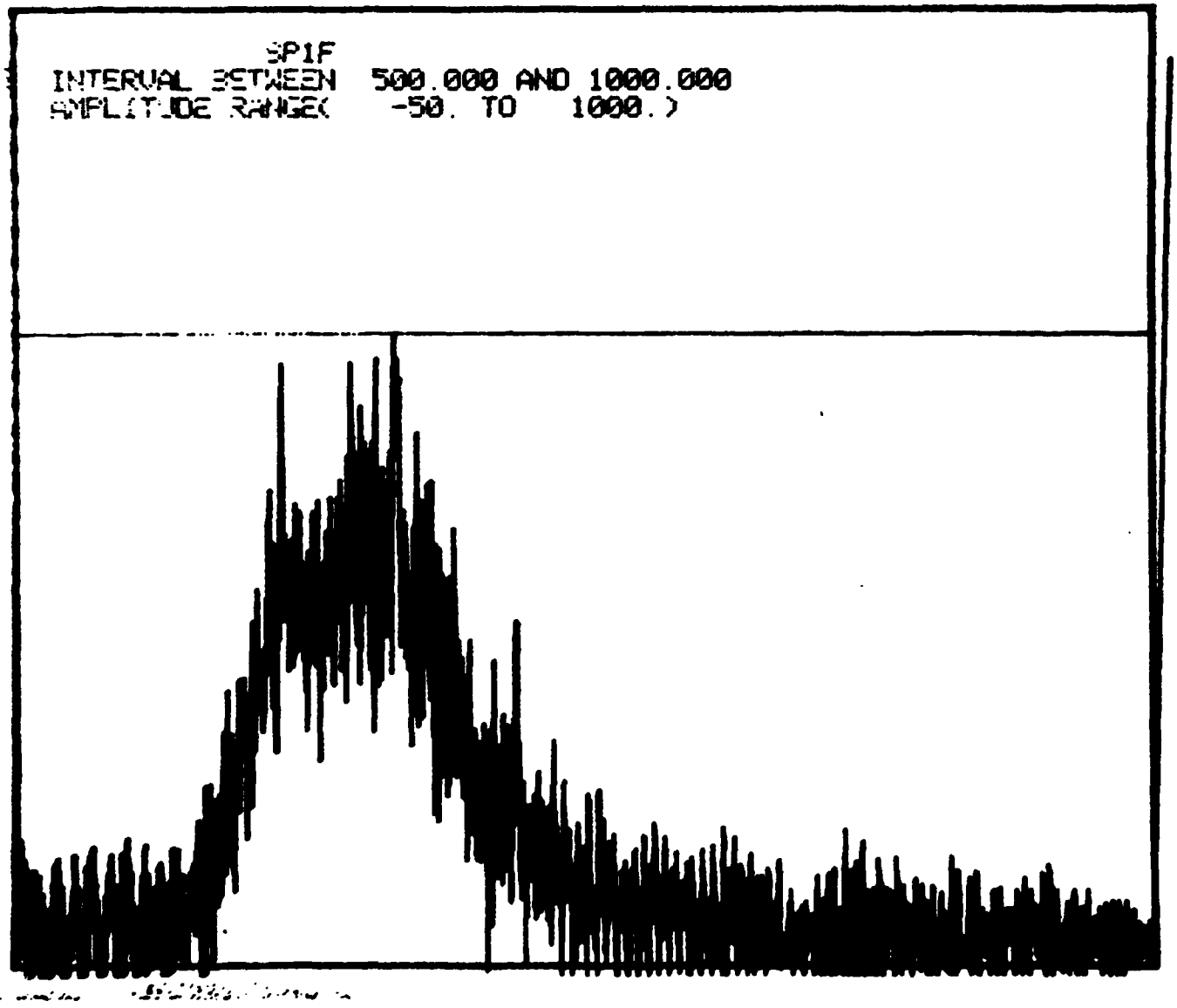
SP1F
INTERVAL BETWEEN 500.000 AND 1000.000
AMPLITUDE RANGE(-50. TO 1000.)

Figure 21

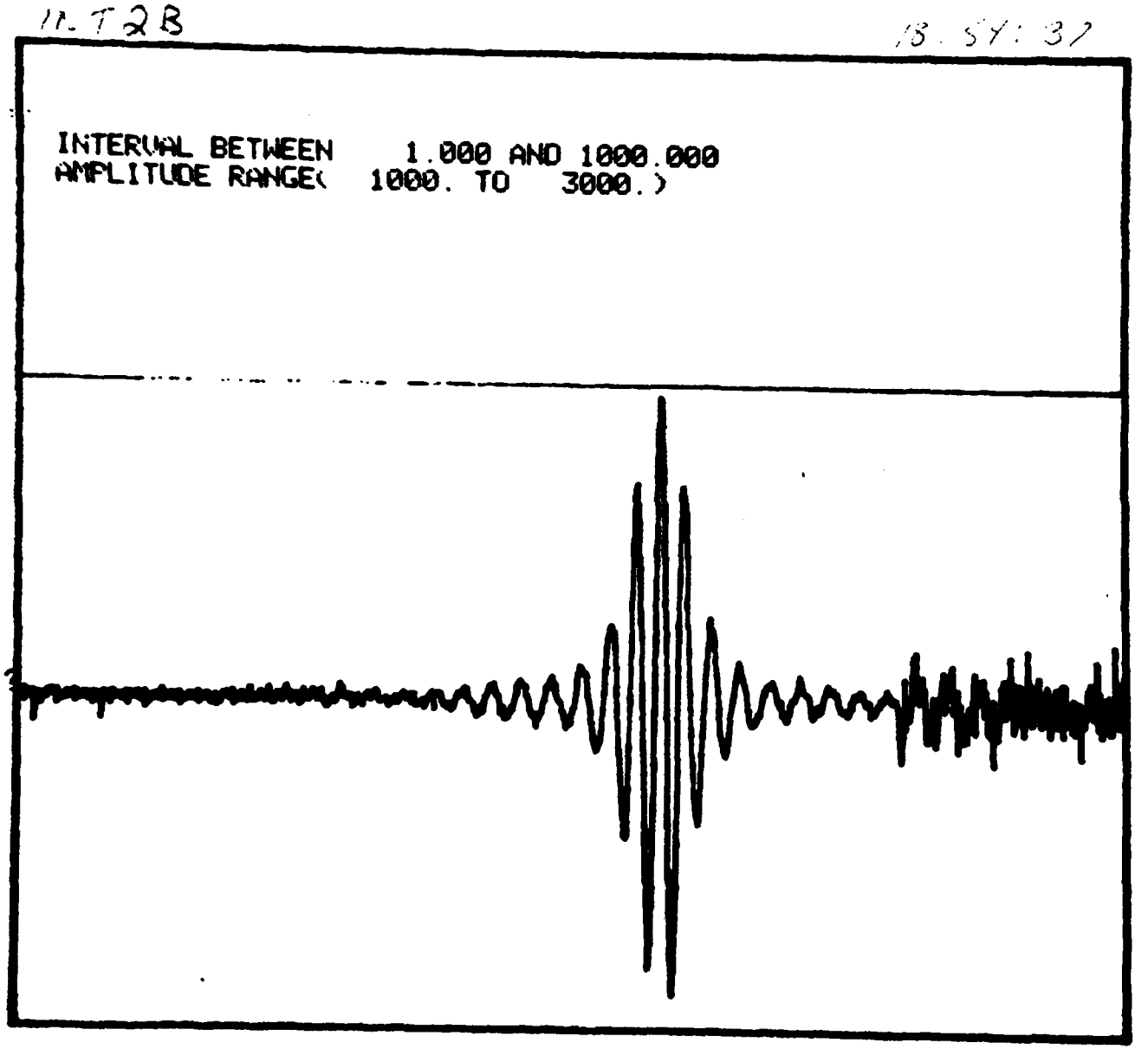
11.T2B
18.SY:37
INTERVAL BETWEEN 1.000 AND 1000.000
AMPLITUDE RANGE(1000. TO 3000.)

Figure 22

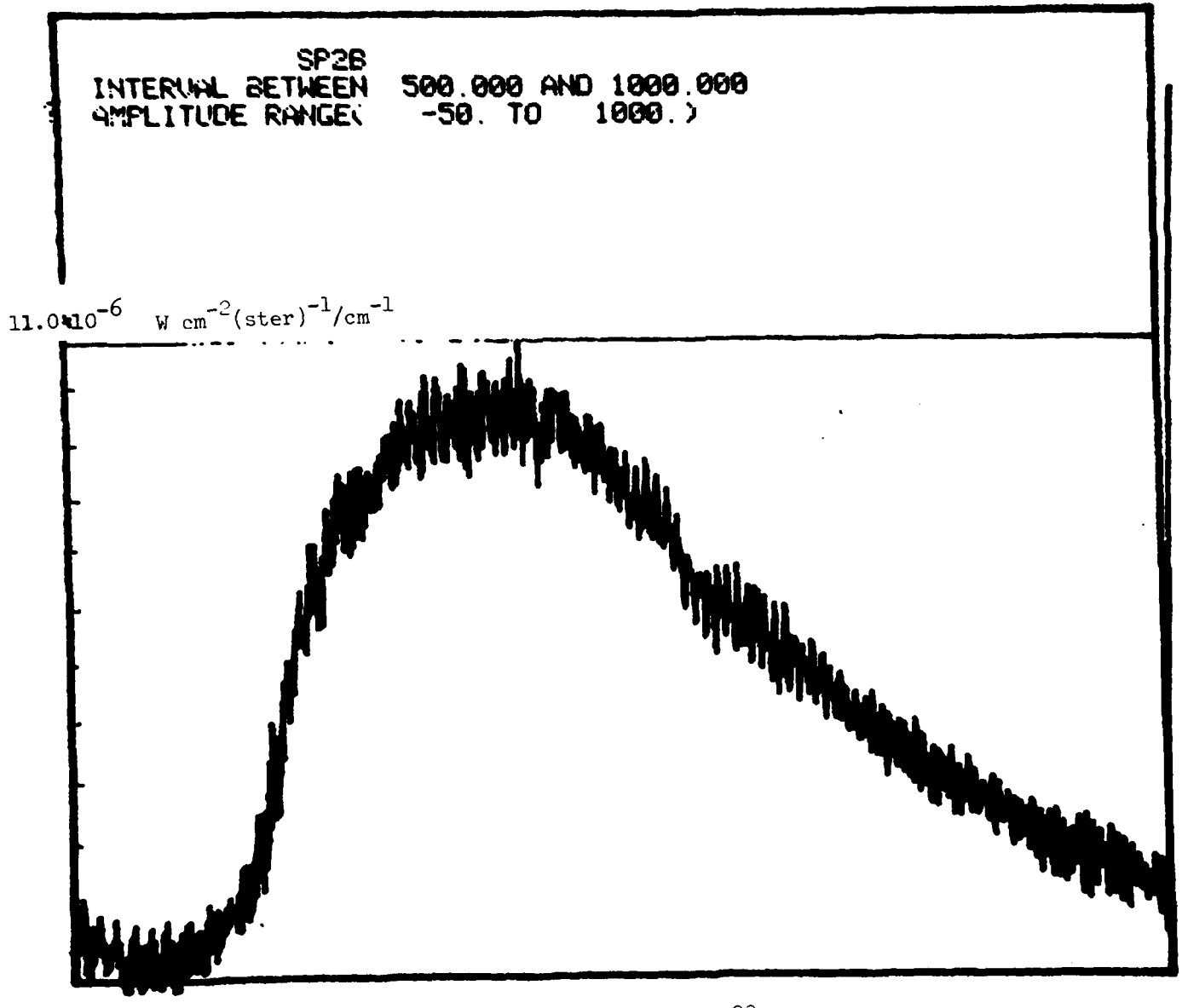
SP2B
INTERVAL BETWEEN 500.000 AND 1000.000
AMPLITUDE RANGE(-50. TO 1000.)
11.0*10^-6 W cm^-2(ster)^-1/cm^-1

Figure 23

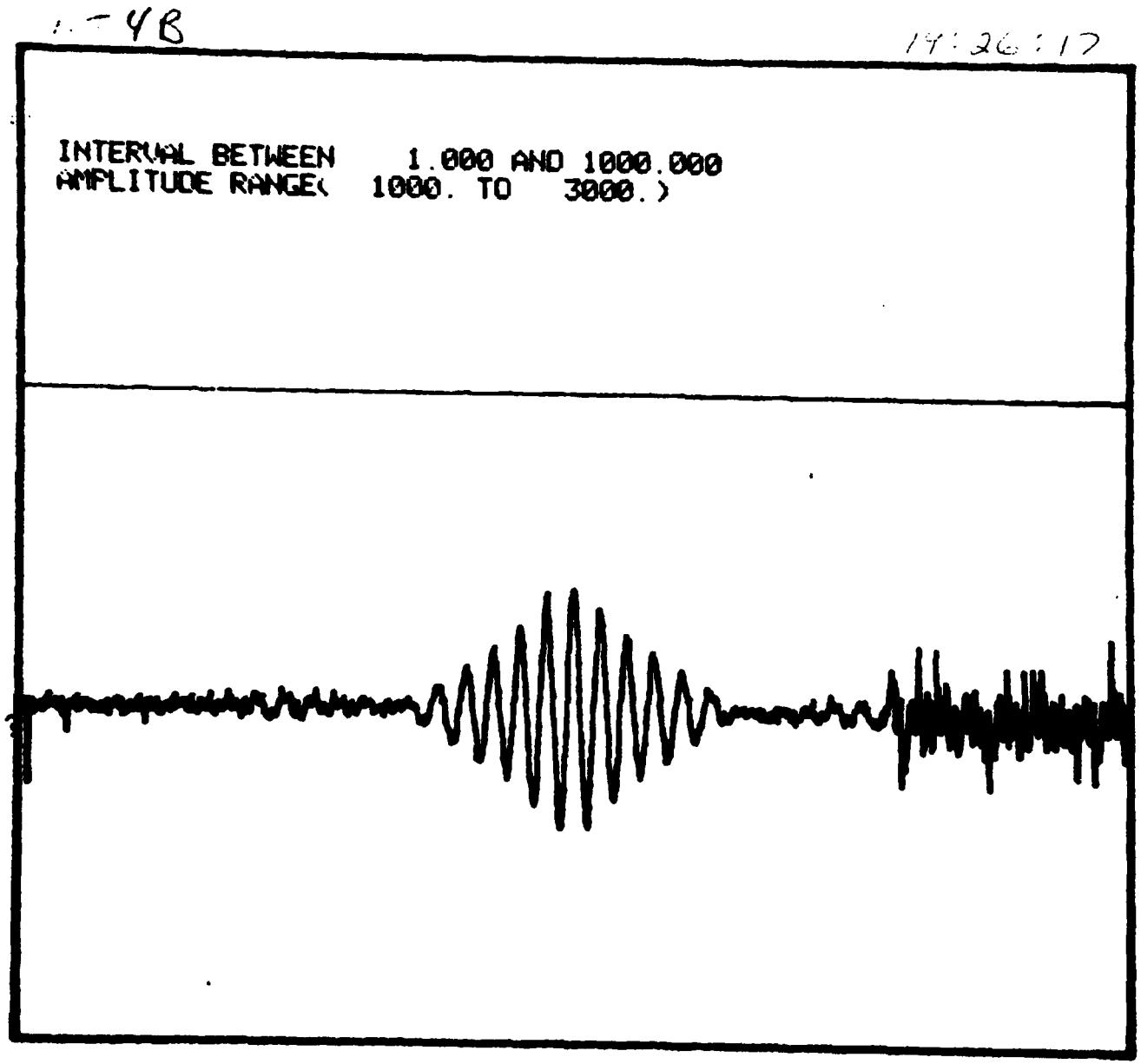
1-4B
14:26:17
INTERVAL BETWEEN 1.000 AND 1000.000
AMPLITUDE RANGE(1000. TO 3000.)

Figure 24

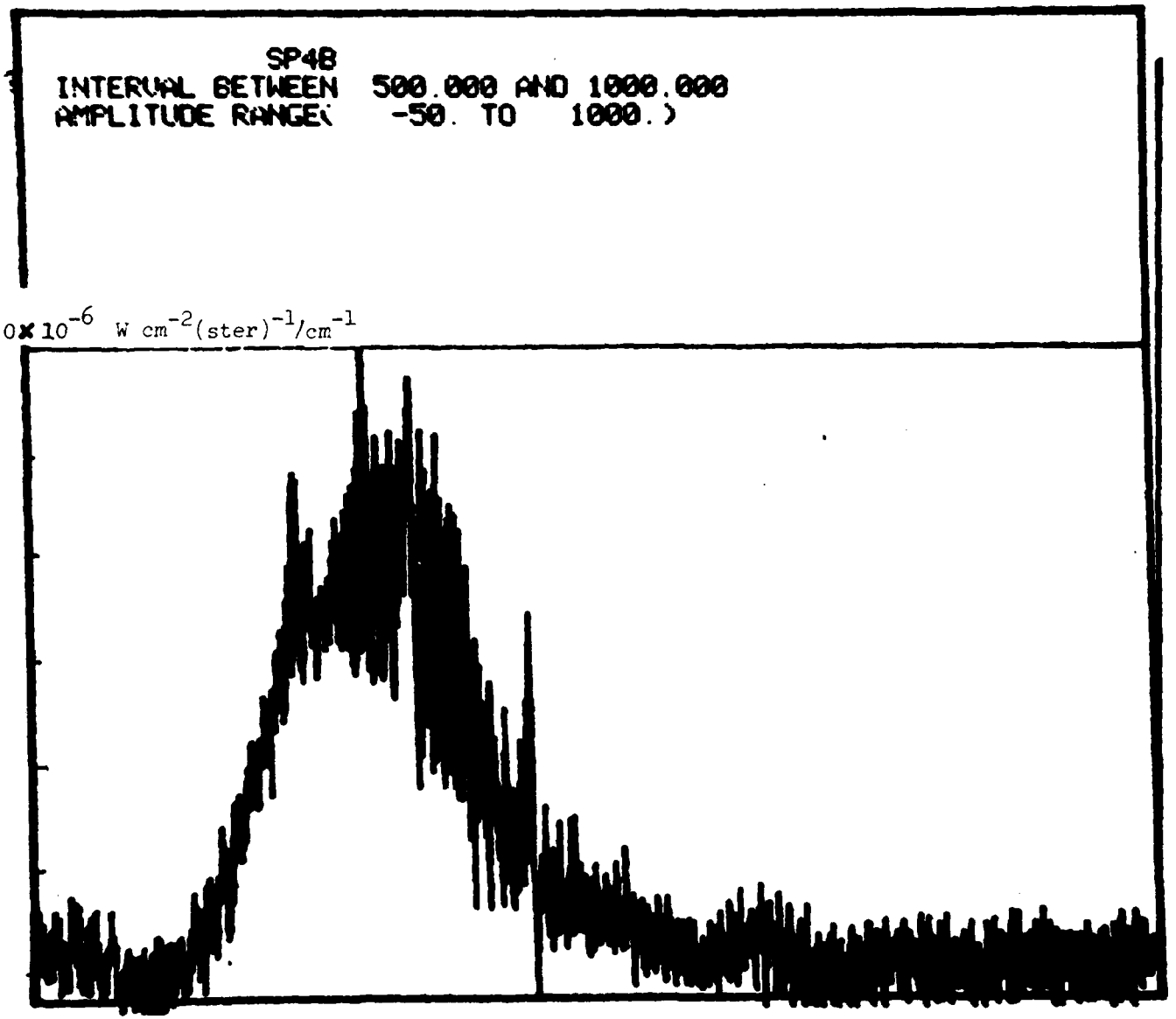
SP48
INTERVAL BETWEEN 500.000 AND 1000.000
AMPLITUDE RANGE(-50. TO 1000.)
6.0✕10^-6 W cm^-2(ster)^-1/cm^-1

Figure 25

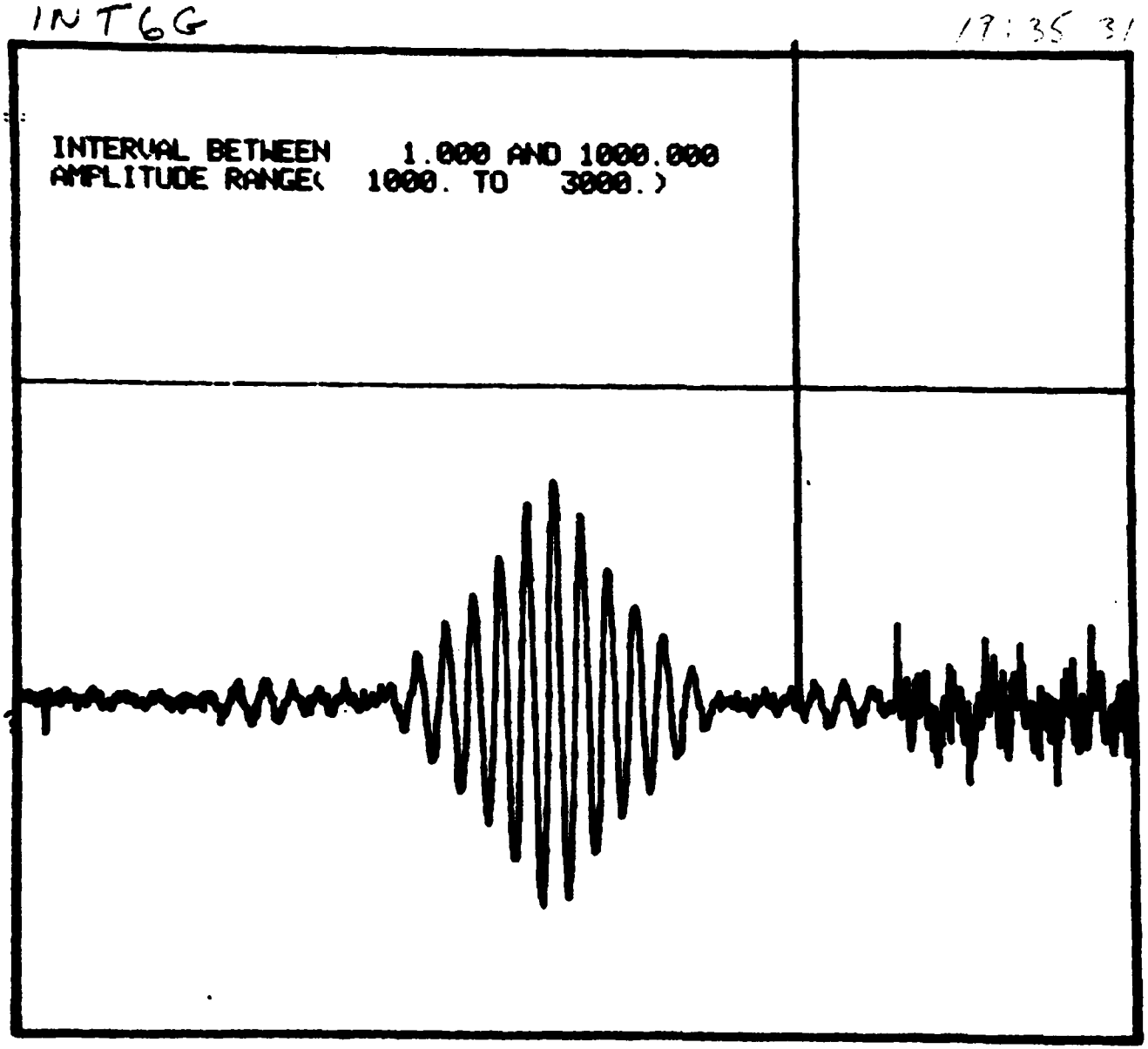
INT6G
19:35 31
INTERVAL BETWEEN 1.000 AND 1000.000
AMPLITUDE RANGE(1000. TO 3000.)

Figure 26

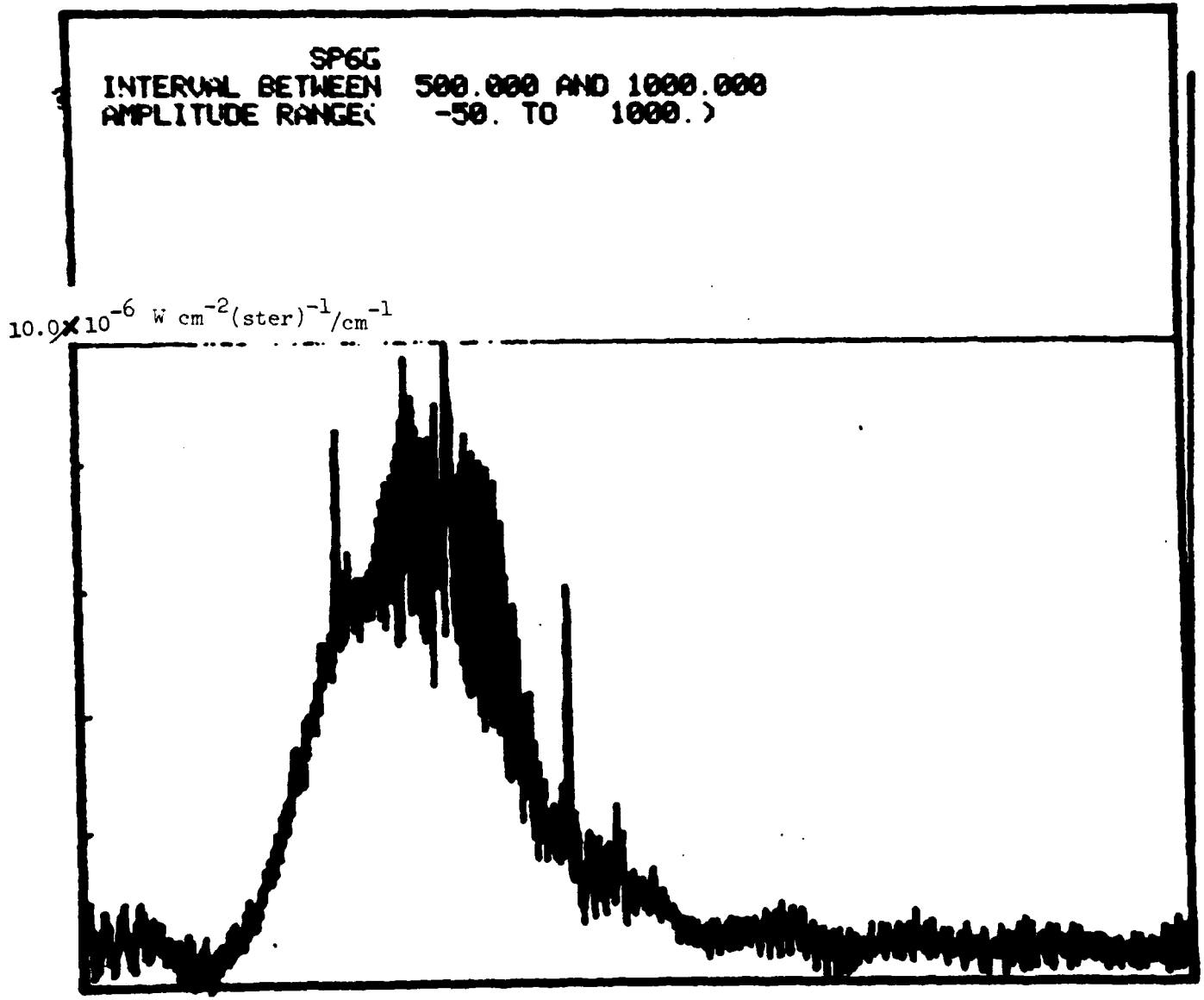
SP6G
INTERVAL BETWEEN 500.000 AND 1000.000
AMPLITUDE RANGE(-50. TO 1000.)
10.0X10^-6 W cm^-2(ster)^-1/cm^-1

Figure 27

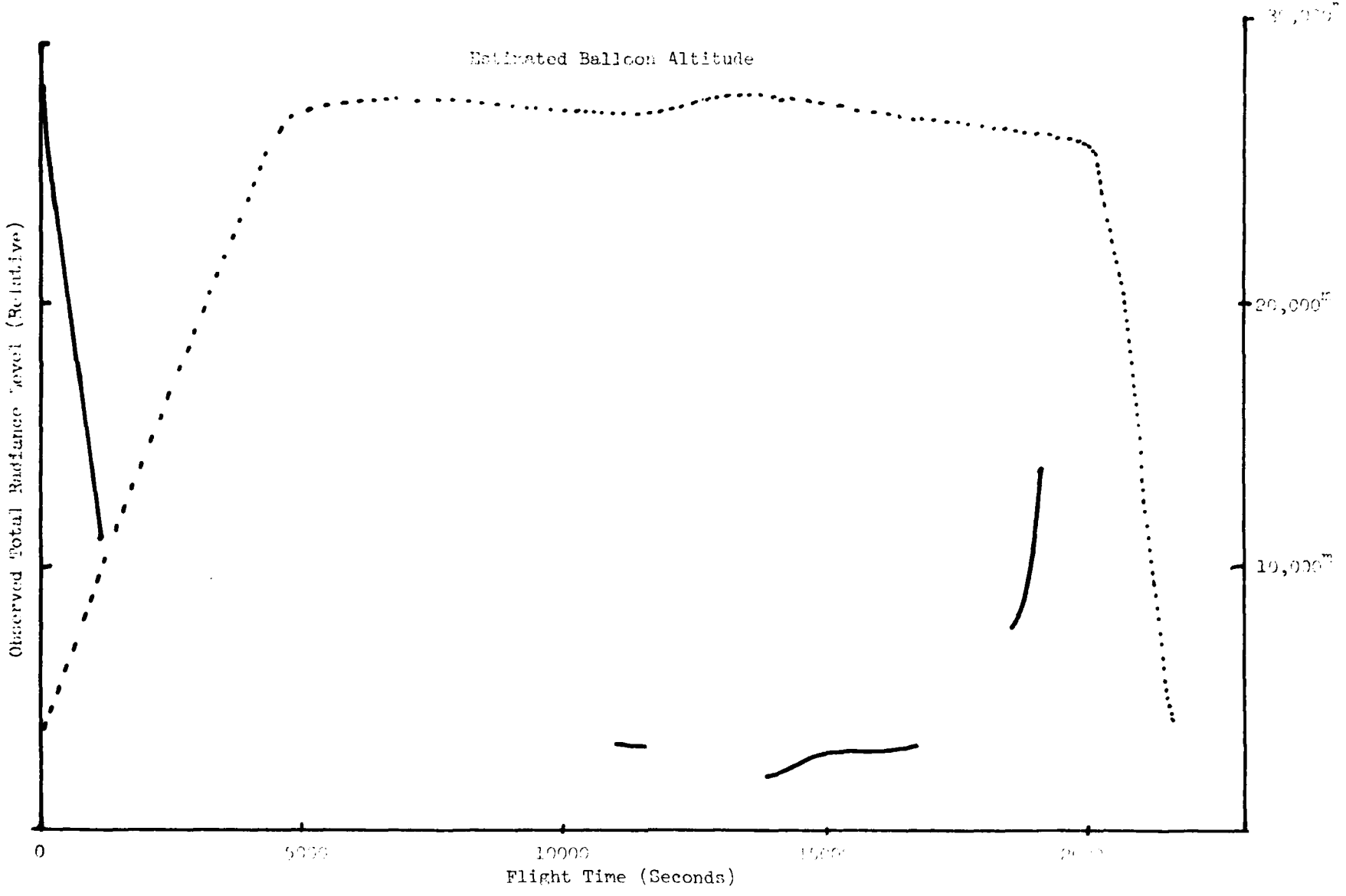

Figure 23 Observed total radiance level and balloon altitude plotted as a function of flight time.

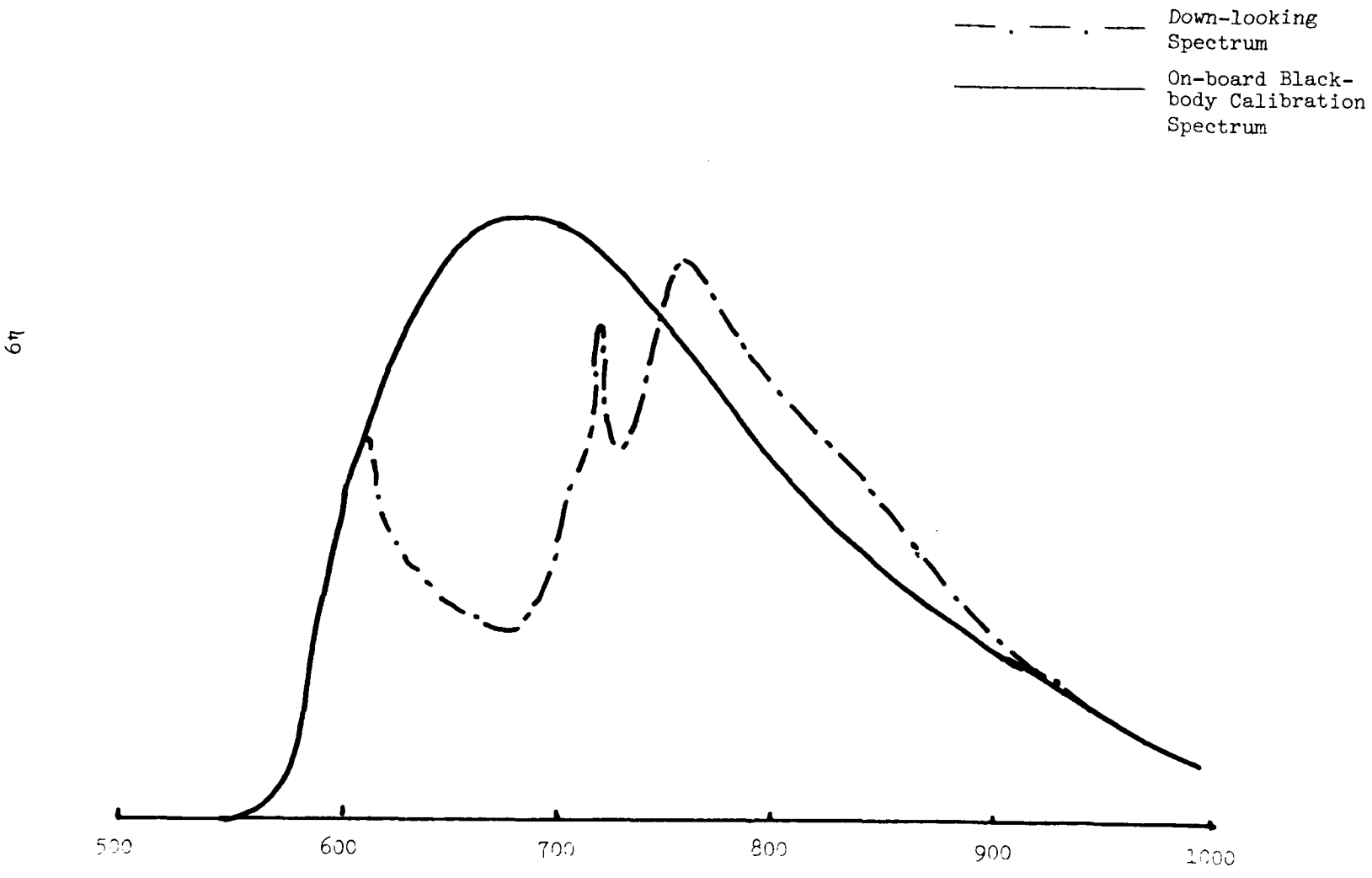

Figure 29 Down-looking spectrum vs. blackbody source calibration spectrum.

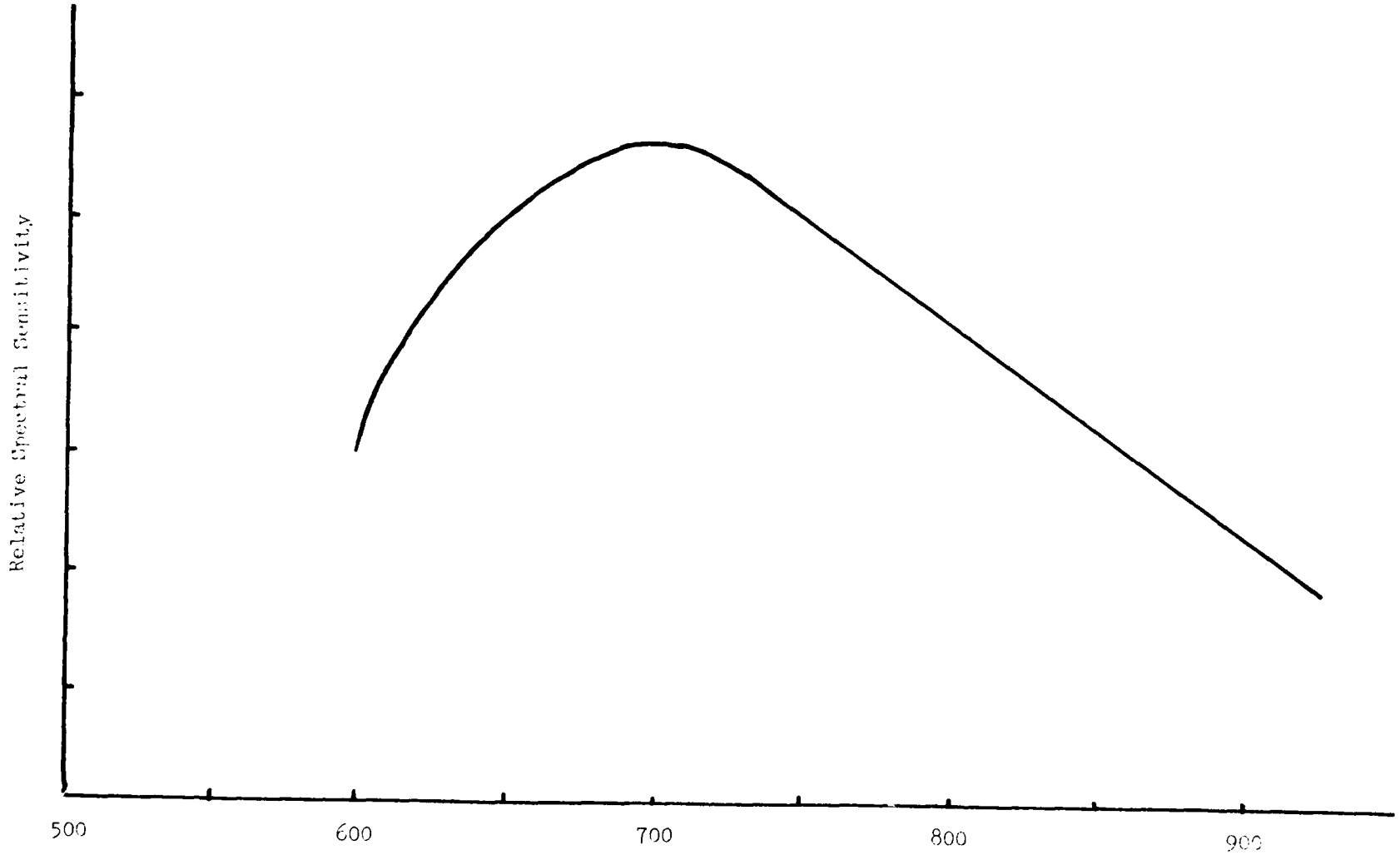

Figure 30 Relative spectral sensitivity of SCRIBE interferometer with Ge:Cu detector.

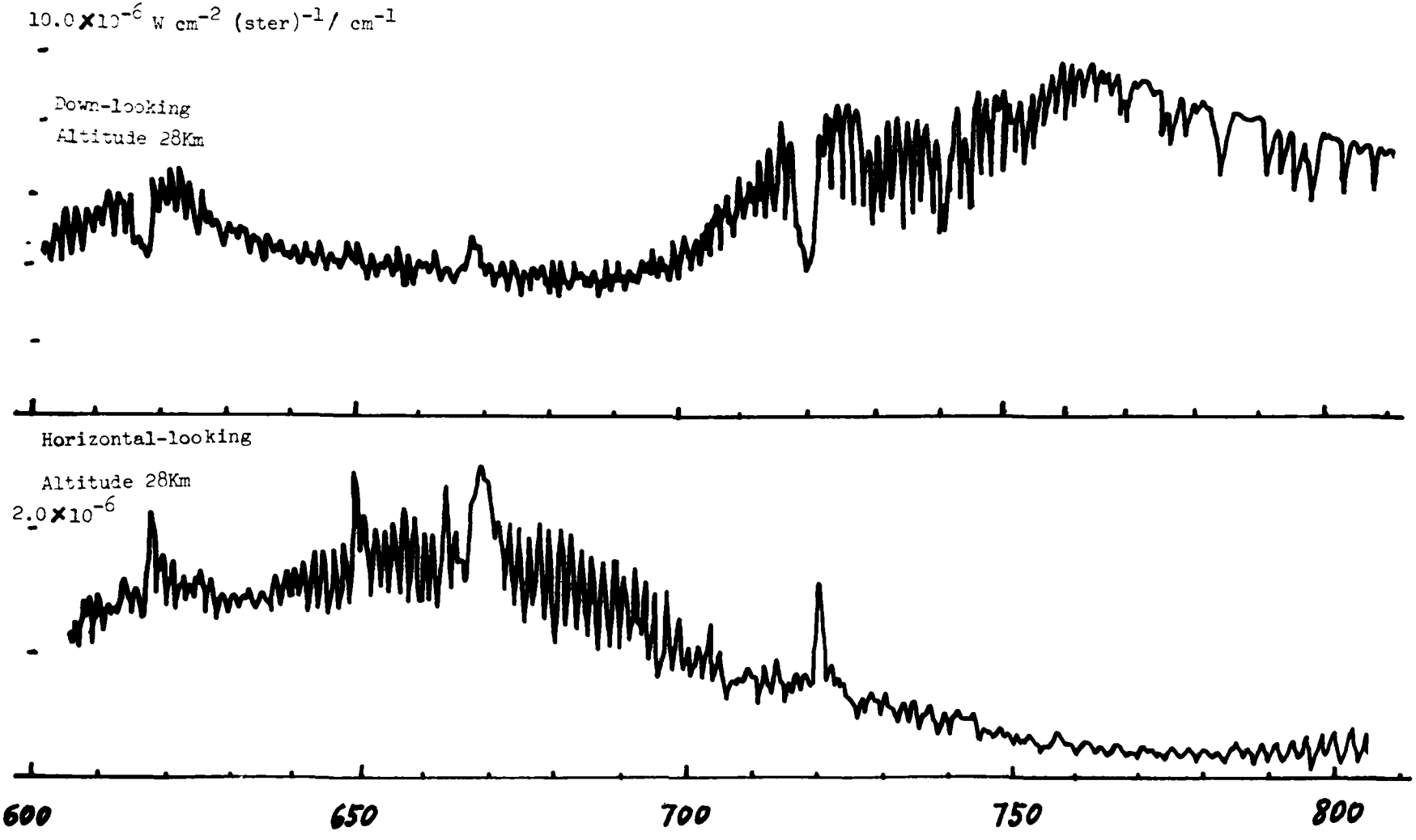

Figure 31

Down-looking spectrum vs. horizontal-looking spectrum.

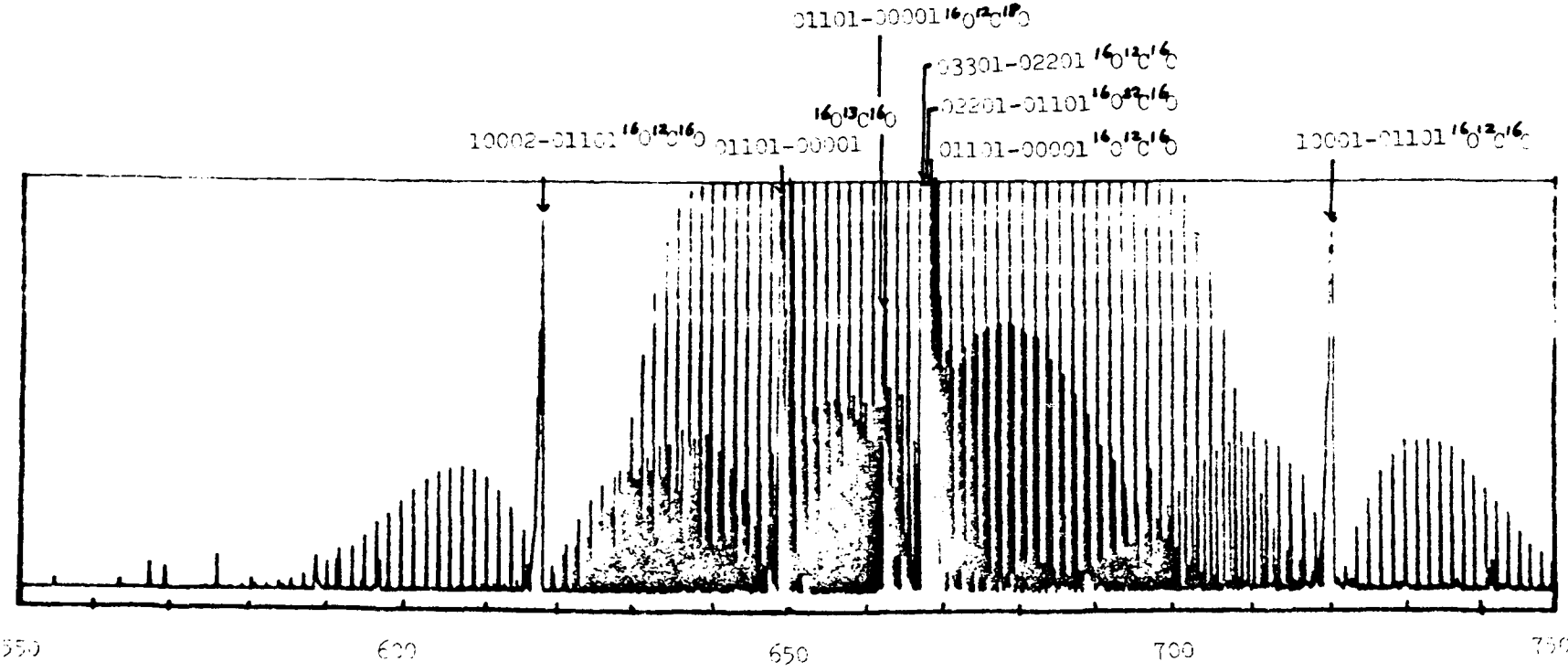

Figure 32 Schematic diagram of the CO_2 bands in the observed 15μ CO_2 transitions.

Figure 33

Synthetic spectrum calculated using FASCODB and AFGL Atmospheric Line Listing.

Molecular total amount

N_2	2.81×10^{24} molecules/cm^2
CO_2	1.19×10^{21}
H_2O	1.05×10^{20}
O_2	7.52×10^{23}

Balloon altitude 30.5 km; elevation angle 3.0°

Scanning function $(\text{sinc})^2$ with hwhm = 0.213 cm^{-1}

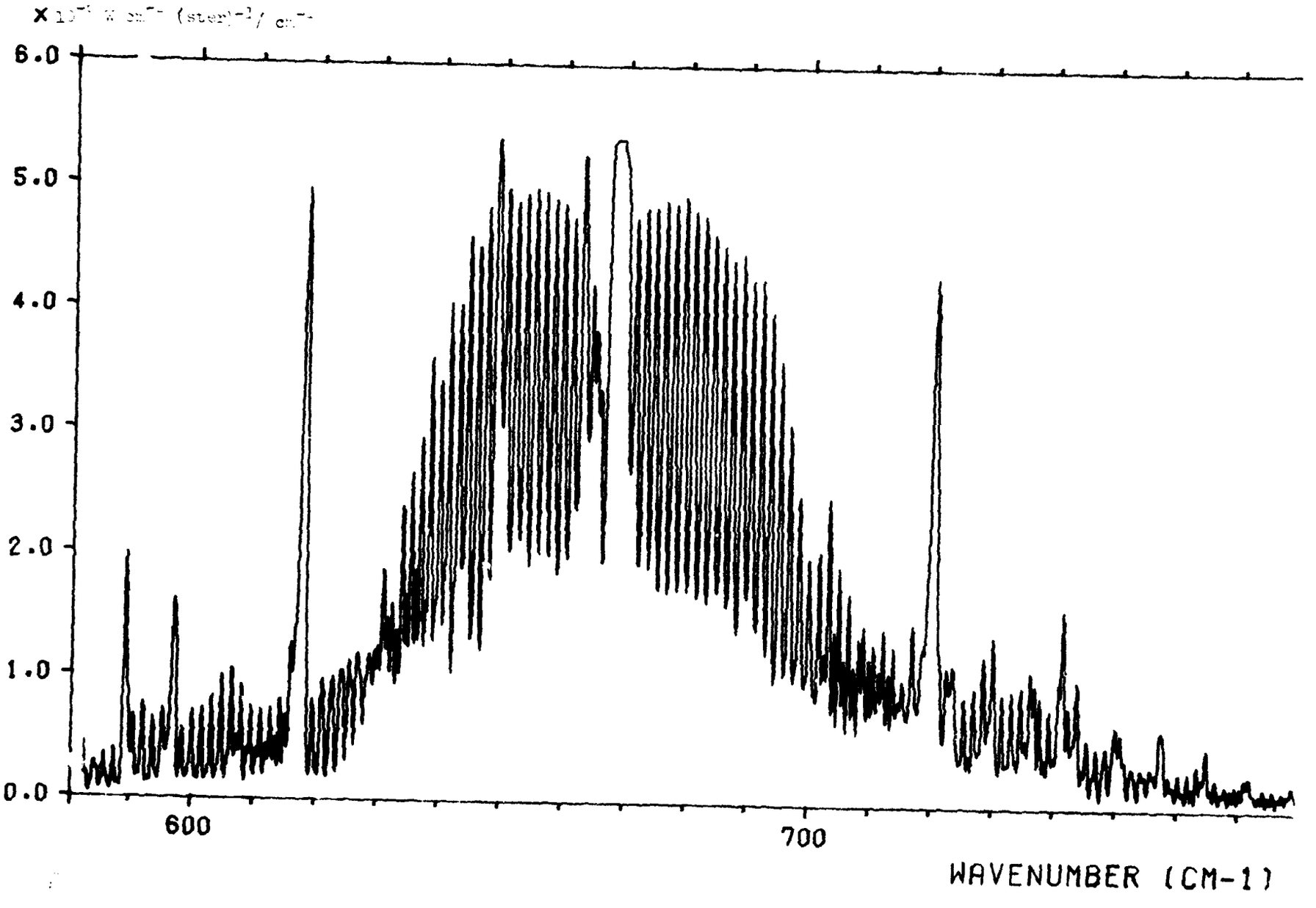
6.0
5.0
4.0
3.0
2.0
1.0
0.0
600
700
WAVENUMBER (CM-1)


DA
FILM
7